To be sure that your preprints are promptly included in the HIGH ENERGY PHYSICS INDEX, send them to (if possible by air mail):

DESY
Bibliothek
Notkestraße 85
2603 Hamburg
Germany

DESY-IfH
Bibliothek
Platanenallee 6
15738 Zeuthen
Germany

DESY 94-215
November 1994

ISSN 0418-9833

Photoproduction Physics at HERA*

B.D.Burow[1], M.Erdmann[2], R.Kaschowitz[3], S.Levonian[4,5], L.Stanco[6]

[1] *Hamburg University, II.Institute of Exp.Physics, Hamburg, Germany*

[2] *Physikalisches Institut, Universität Heidelberg, Germany*

[3] *III.Physikalisches Institut der RWTH, Aachen, Germany*

[4] *DESY, Hamburg, Germany*

[5] *Lebedev Physical Institute, Moscow, Russia*

[6] *Dipartimento di Fisica dell' Universita and INFN, Padova, Italy*

*Invited contributions to the Workshop on Two-Photon Physics at LEP and HERA, Lund, Sweden, May 26-28 1994.

Introduction and Overview to Photoproduction Physics at HERA

Martin Erdmann

Universität Heidelberg, Physikalisches Institut

Abstract:

The photon looks very much like a hadron.

But the photon is not a hadron.

1 Photons of the HERA microscope

The HERA collider at DESY is todays largest electron-proton microscope: in the Coulomb field of the proton the electron emits a photon which illuminates the proton (fig.1). The resolution power of this microscope depends on the photons four-momentum transfer $Q^2 \equiv -q^2$ which varies primarily with the angle of the scattered lepton. HERA covers the extreme range of 13 orders in Q^2 from 10^{-8} to 10^5 GeV^2 and provides large center of mass (CM) energies for the photon-proton system up to $\sqrt{s_{\gamma p}} \leq 300$ GeV.

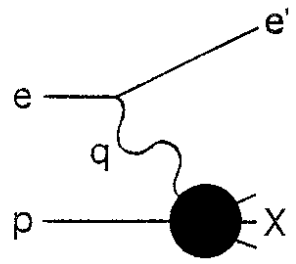

Figure 1: ep scattering at HERA.

At small scattering angles of the lepton, the emitted photon is quasi-real. Here the photon becomes the particle of interest: the photon has never been explored before at such high CM energies as are available at HERA.

For this workshop we divided the HERA results on the photon into 1+4 chapters:

- introduction and overview,
- total γp cross section and its contributions (Burkhard Burow),
- direct versus resolved photon interactions and charm production (Luca Stanco),
- partons of the photon (Richard Kaschowitz), and
- hard scattering in events with a rapidity gap (Sergey Levonian).

2 The picture of the photon

2.1 Photon-proton processes

From previous fixed target experiments we know that the photon does not necessarily interact directly as a gauge boson. It rather exhibits a hadronic type of scattering which can be explained by the photons fluctuation into a vector meson before it scatters off the proton (vector meson dominance model VDM [1],[2]). The picture of photon-proton scattering is therefore very similar to the one of hadron-hadron scattering. Several different processes contribute:

- the peripheral scattering of two extended objects consists of elastic, single and double diffractive scattering and the soft part of non-diffractive inelastic interactions.
- hard non-diffractive inelastic interactions include the (rare) hard scattering of two partons of the beam particles which result in a final state with large transverse energy. The parton-parton scattering can be described by QCD theory. If the photon interacts after forming a vector meson i.e. a hadron-hadron kind of scattering, the process is refered to as *VDM resolved* hard scattering.

The pointlike coupling of the photon to electric charge allows for two hard processes beyond what is seen in hadron-hadron scattering:

- the photon itself couples to a parton of the proton (*direct* processes),
- the photon can split into a $q\overline{q}$ pair without any means of a bound state before interacting with the proton (*anomalous resolved* process).

All these processes are accessible to the HERA experiments. A theoretical review of the different contributions to photon-proton interactions can be found e.g. in [3], which uses a language widely spread at HERA.

2.2 Parton distributions

To predict the hard parton-parton scattering in photoproduction processes, information on the parton distributions of the proton and the photon are needed. The structure of the proton has been well measured in the relevant kinematic range in deep inelastic lepton-nucleon scattering. In the case of the photon, the pointlike contributions (anomalous resolved and direct) can be calculated in perturbative QCD, but not the VDM resolved photon part where the $q\overline{q}$ pair forms a bound state. Therefore the concept of a photon structure function has been introduced for the resolved contributions which is to be measured by experiments. It includes the VDM and the anomalous processes, since they are coupled in the evolution equation of such a structure function [4].

Two-photon $\gamma\gamma$ experiments at electron-positron colliders have determined the photon structure function F_2^γ which provides information on the quark content of the photon. The measurements cover quark momenta in the range $0.007 \leq x_\gamma \leq 1$ [5]. F_2^γ is large at high x_γ due to the anomalous contribution and looks different from a hadronic structure function [6]. The measurements constrain the quark distributions reasonably well, but give only weak constraints on the gluon of the photon, such that a variety of parametrizations for the photon structure was suggested from these data as shown in fig.2. Recently the gluons of the photons were studied in hard collisions of two real photons at e^+e^- colliders showing that the gluon content is not very large at x_γ closed to unity [7].

In hard photon-proton scattering at HERA the partons of the proton probe both the quark and gluon contents of the photon. These interactions provide for the first time direct information on the gluon in the photon at low x_γ.

2.3 QCD matrix elements

In leading order QCD the hard interactions are viewed as elastic parton-parton scattering. The combinations of 2 partons with different quantum numbers (quarks, gluons, photon) lead to different matrix elements M which determine the angular distribution of the scattered partons (e.g.[9]). In fig.3 the shapes of several matrix elements are shown as function of the scattering angle Θ^* in the CM system of the two partons. The distributions were normalized to 1

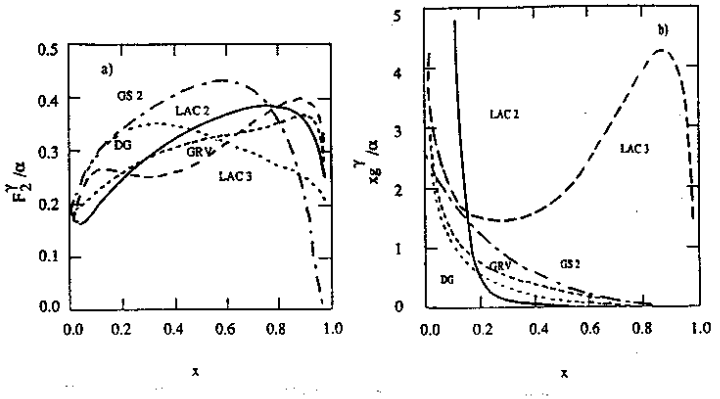

Figure 2: Quark and gluon distributions in the photon from different sets of parametrizations with e^+e^- data as input (from [8]).

at $\cos\Theta^* = 0$ and do not distinguish between forward ($\Theta^* \leq 90°$) and backward ($\Theta^* \geq 90°$) scattering. All distributions rise towards small scattering angles. The resolved photon contributions which give the largest rates rise much faster compared to the direct photon processes: the distribution of the parton scattering angle can therefore be used to separate direct and resolved photon contributions.

3 Detectors and data taken

The two large detectors H1 [10] and ZEUS [11] are well described in the literature. They have been designed as general purpose experiments. The interaction point is surrounded by tracking systems which are located inside a strong magnetic field. Large calorimeters - liquid argon and lead scintillator (H1), and uranium scintillator (ZEUS) - cover the entire stereo angle down to the beam pipe. Muon detectors surround the tracking and calorimeter systems. A separate magnetic spectrometer for muons is provided in the direction of the outgoing proton. In the same direction, close to the proton beam, a spectrometer has been installed to tag events where the proton scatters under very small angles.

Luminosity is determined with the Bethe-Heitler process $ep \to e\gamma p$. To measure the electron and the photon two calorimeters were positioned close to the beamline 30m respectively 100m away from the interaction point in the direction of the scattered electron.

The integrated luminosity used for physics analysis in 1993 was of the order of several hundred inverse nanobarn. This corresponds to an order of 10^6 ep events which are mostly photoproduction processes due to the large cross section.

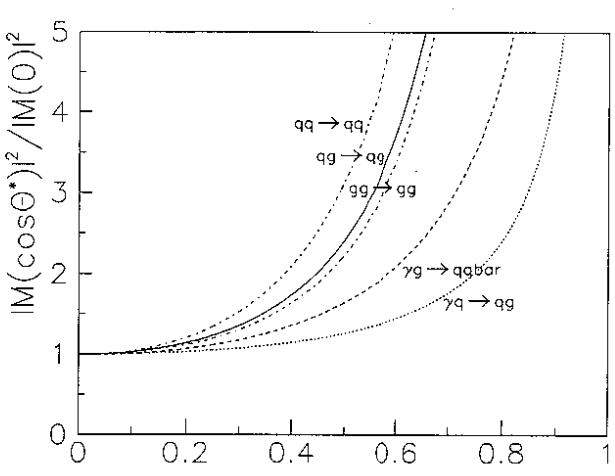

Figure 3: Matrix elements of different leading order parton-parton processes versus the scattering angle in the parton-parton CM system. All curves were normalized to 1 at $\cos\Theta^* = 0$. The distributions of the three resolved photon processes which dominate the jet rates rise more steeply towards small scattering angles compared to the direct photon processes (dotted: QCD Compton, dashed: Photon-Gluon-Fusion).

4 Final state variables and event kinematics

Common kinematic variables of particles or jets in the final state are shown in fig.4:

- **the transverse momentum** p_t: since the photon is almost parallel to the incoming electron direction, p_t is measured wrt. the beam axis.
- **The azimuthal angle** Φ is measured in a plane perpendicular to the beam axis.
- **The polar angle** Θ is measured wrt. the outgoing proton. The pseudo-rapidity is defined accordingly as $\eta = -\ln\tan\Theta/2$.

As a consequence of the largely different beam energies (protons $E_p = 820$GeV, leptons $E_e = 26.7$GeV) particles which scatter 90^o in the γp-CM system appear typically in the laboratory frame at rapidity $\eta \approx 2$. Therefore the HERA detectors measure mainly the particles in the photon hemisphere over a large range of ~ 5 rapidity units and cover ~ 2 rapidity units of the proton hemisphere.

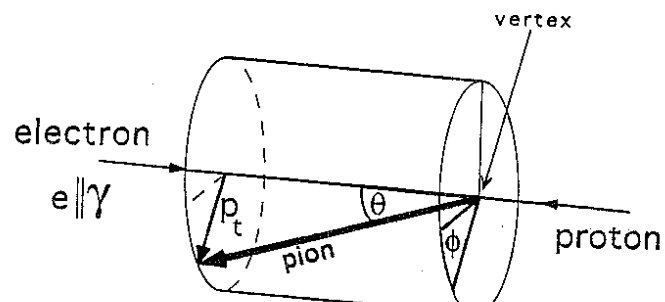

Figure 4: Variables for the final state: since the quasi-real photons are essentially parallel to the electron direction, the transverse momenta p_t of particles are measured wrt. the beam axis. The polar angle Θ is determined relative to the proton beam direction. The azimuthal angle Φ is measured in a plane perpendicular to the beam axis.

For events with 2 jets in the final state, **the momentum fraction of the parton from the photon** x_γ can be approximately reconstructed by

$$x_\gamma = \frac{E_{t_1} e^{-\eta_1} + E_{t_2} e^{-\eta_2}}{2E_\gamma} \qquad (1)$$

where $E_{t,i}, \eta_i$ are the transverse energy and the pseudo-rapidity of the two jets and E_γ is the energy of the photon. For direct photon processes the entire γ energy is available to the hard process such that the true x_γ is $x_\gamma = 1$.

Three scales are important to characterize the kinematics of events from HERA photoproduction physics (fig.5):

- **the four momentum transfer of the photon** $Q^2 \equiv -q^2$: it can be determined from the lepton beam energy E_e and the energy E'_e and scattering angle Θ of the scattered lepton: $Q^2 = 4E_eE'_e\sin^2((\pi-\Theta)/2)$. Large Q^2 up to the kinematic limit of $Q^2 = s_{ep}$ is considered as the deep inleastic scattering (DIS) regime. The transition to the photoproduction region is theoretically expected to be of order $Q^2 \approx$ a few GeV^2. Without precise theoretical guidance at HERA we use an experimental definition of the transition region: if the electron is detected in the main detectors we call the event DIS, if not, we call it a photoproduction event. The limit is at $Q^2 \approx 4$GeV^2.
- **The CM energy available in the photon-proton system** $s_{\gamma p}$: the variation of the photon energy can be expressed in terms of the scaled variable $0 \le y \le 1$ which connects the ep and the γp CM energies $s_{\gamma p} = y s_{ep} \le 300^2$GeV^2. $y \equiv pq/pe$ is calculated from the four vectors of the proton p, photon q and beam electron e. The photon vector can be determined from the final state hadrons X as $q = X - p$. On the lepton side, y can be precisely measured as $q = e - e'$, if the scattered lepton e' is tagged in the luminosity system, that is inside the acceptance window $[0.2 \le y \le 0.8, Q^2 \le 0.02$ GeV$^2]$.

  For CM energies below $\sqrt{s} \sim 40$GeV proton-gas interactions from the interaction region are a serious background. It can be suppressed by intelligent cuts on the energy flow distribution of the events. Above $\sqrt{s} \sim 40$GeV this background can be neglected.

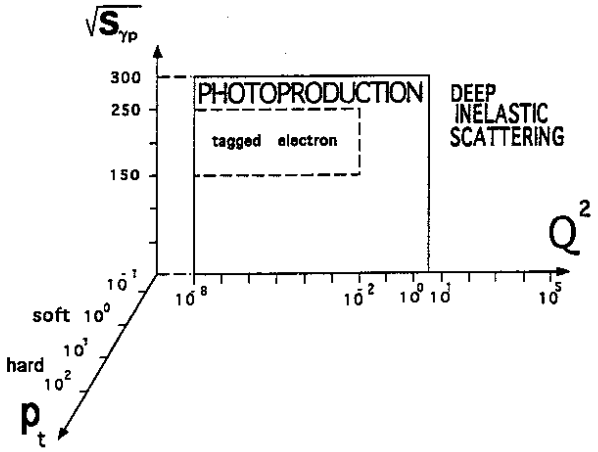

Figure 5: Scales in ep scattering: the squared four momentum $Q^2 \equiv -q^2$ of the photon separates the deep inelastic scattering region from the photoproduction region. $\sqrt{s_{\gamma p}}$ is the CM energy available in the γp system. The transverse momentum scale P_t distinguishes soft from hard scattering reactions.

- **The transverse energy of the event P_t**: the experiments trigger events with single tracks of transverse momentum $p_t \geq 0.1$GeV and events with transverse energy deposited in the calorimeter of order $E_t \approx 100$GeV. There is a transition region from soft to hard scattering which can be determined experimentally (see below). QCD calculations of hard γp processes use (a multiple of) P_t as the relevant scale parameter.

5 The total photon-proton cross section

One of the first HERA results was the determination of the total photon-proton cross section [12, 13]. When compared to the previous measurements at one order of magnitude less CM energies no dramatic rise of the cross section is observed (fig.6). This was expected e.g. by Pomeron exchange models (e.g.[14]): the modest rise is very similar to the rise of the cross section in hadron-hadron scattering.

A further similarity between scattering of photons and hadrons comes from the relative contribution of non-diffractive processes to the total cross section: according to a study by Gotsman this ratio is $\sim 60\%$ in $\overline{p}p$ scattering independent of the CM energy (fig.7) [15]. The measurement by ZEUS gives a ratio $R = 64 \pm 4\%$ [12] which has been introduced in the same figure.

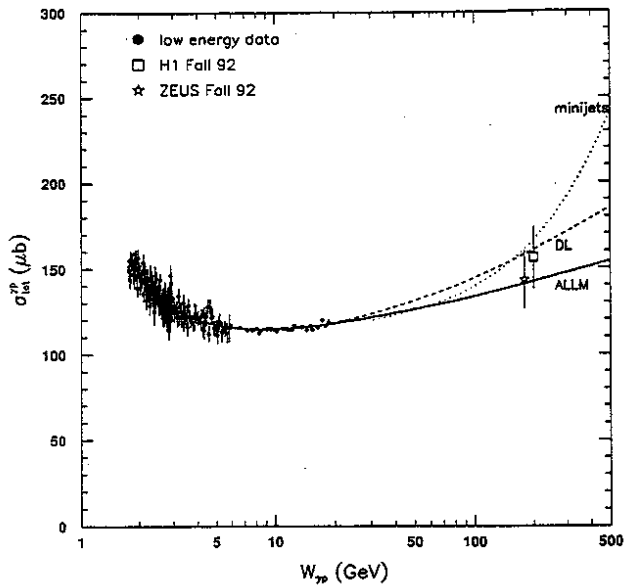

Figure 6: Energy dependence of the total cross section in quasi-real photon-proton interactions.

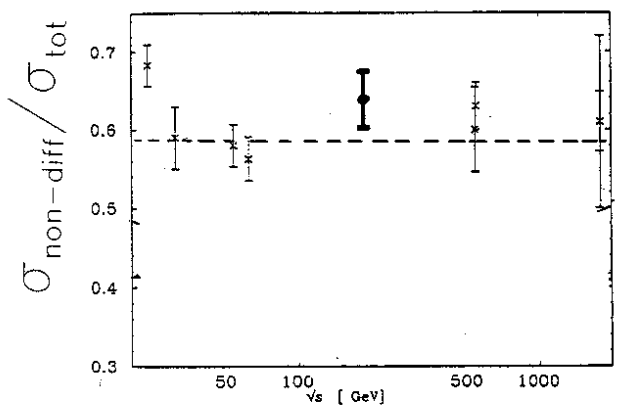

Figure 7: Energy dependence of the non-diffractive inelastic scattering contribution relative to the total cross section in $\overline{p}p$ (crosses) and γp (point: ZEUS) scattering.

6 Charged particles

Charged particles with large transverse momenta reflect hard photon-proton interactions. In fig.8 the H1 measurement of the ep differential cross section $d\sigma^2/d\eta/dp_t^2$ [16] is compared to $\overline{p}p$ data of the UA1 experiment at the same CM energy $\sqrt{s} = 200$GeV [17]. The UA1 data have been normalized to the level of the H1 data at $p_t = 1.5$ GeV: the corresponding down-scale factor for the $\overline{p}p$ data can well be explained within the VDM picture.

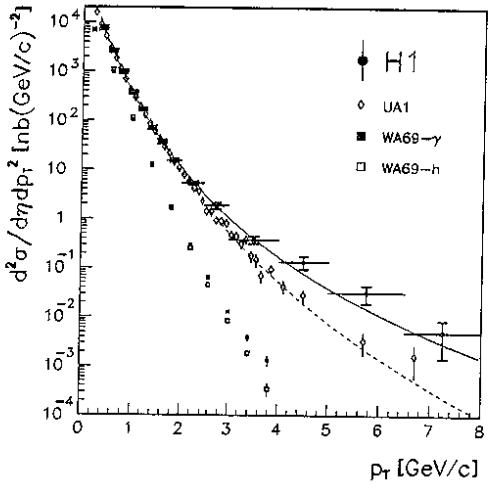

Figure 8: Charged particle differential cross sections for photon-hadron scattering compared to the shape of hadron-hadron scattering: γp data (H1, full circles) at $\sqrt{s} = 200$GeV exceed in the high p_t region the $\overline{p}p$ data (UA1, open diamonds) at the same CM energy. Results from a fixed target experiment (WA69) at $\sqrt{s} = 18$GeV show a similar difference between γp (full rectangles) and hadron-p (open rectangles) data.

In the low p_t region the shapes of the cross sections of photon and hadron data are very similar: the photon behaves like a hadron. At transverse momenta above $p_t \geq 4$GeV the photon data exhibit a harder spectrum compared to the hadron data.

A similar difference between photon and hadron scattering has been observed in the fixed target experiment WA69 [18] at $\sqrt{s} = 18$GeV: they could switch between photon and hadron beams and demonstrated the difference between photon-proton and hadron-proton interactions (fig.8). However, the low CM energy did not enable them to draw strong conclusions on the origin of this effect.

The excess of the γp over the $\overline{p}p$ data at $\sqrt{s} = 200$GeV is significantly larger than a simple comparison of a 2 quark (photon) versus a three quark object (antiproton) would give. Also the variation of the photon beam energy compared to the fixed $\overline{p}$ energy can not explain this difference. The most likely explanation for this excess are the anomalous and direct processes of γp interactions which are absent in the case of $\overline{p}p$ scattering.

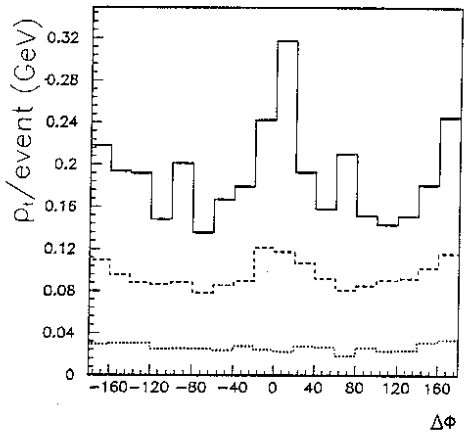

Figure 9: Azimuthal energy flow of charged particles wrt. the particle with the leading transverse momentum (H1 data). This particle is excluded from the distribution. The histograms show the distribution depending on the total transverse energy measured in the calorimeter: $E_t \leq 5$GeV (dotted), $E_t \geq 10, 20$GeV (dotted, full).

7 Transition from soft to hard scattering: the formation of jets

The transition region from the soft peripheral scattering of two extended objects to the regime of partonic hard scattering can be studied by a search for large local energy depositions (jets). In fig.9 the transverse energy flow of charged particles is shown versus the azimuthal angle relative to the particle with the largest transverse momentum. The particle itself is excluded from the distribution.

The figure shows the development of the energy flow as a function of the transverse energy E_t^{calo} measured in the H1 calorimeter: at $E_t^{calo} \leq 5$GeV (dotted line) no structure is seen in the distribution; the events are spherical in the transverse projection as one would expect from soft scattering type of events. For $E_t^{calo} \geq 10$GeV (dashed line) the particles start focussing around and opposite to the leading p_t particle. The effect is even more pronounced for measurements in the calorimeter above $E_t^{calo} \geq 20$GeV (full line): these local and large energy deposits exhibit jet formation which reflect the underlying hard scattering of partons.

8 Jet algorithms

Most of the HERA photoproduction analyses use a cone type algorithm for the jet search. Cone algorithms follow the recommendations of the *snowmass accord* [19] and use a 2 dimensional grid of the pseudorapidity η and azimuthal angle Φ. The size of the cone is typically $R = \sqrt{\Delta\eta^2 + \Delta\Phi^2} = 1$, or $R = 0.7$, with the requirement of a minimal transverse energy deposited inside the cone. The cones cut out clearly defined areas around local energy deposits which can sit on top of some global energy flow in the event. With this feature, the cone algorithm is well suited for jet search in a hadron-hadron scattering environment such as resolved photoproduction.

Jet cluster algorithms are used in addition, such as the jade algorithm or the k_t algorithm. They are well suited for studying properties of the photon remnant particles because these algorithms allow for the formation of jets from energy deposits around the beam hole.

9 Jets and partons

The very first jet data at HERA showed a general behaviour as expected from QCD. With the high statistics collected since, we want to learn more on the underlying parton scattering. The central question is how do the measured observables correlate with the parton quantities?

Leading order QCD monte carlo generators (Herwig [20], Pythia [21]) are available to study these correlations. They contain the LO 2 parton scattering processes, parton showers and fragmentation to the hadron level, and are processed all the way through to the detector observed quantities. With these programs, predictions on the jet-parton correspondence can be explored.

Before these jet-parton correlations from a generator can be applied to data, it is mandatory that the local energy flow around the observed jets (*jet profiles*) are checked versus the predicted energy flow in the monte carlo. Any deviation adds to the uncertainty in the translation from data observations to the partons and therefore washes out conclusions on the parton scattering.

The following comparisons between jets found in data and generated events are based on a cone jet algorithm using the cone size $R = 1$. In fig.10a the transverse energy flow per event is shown in a Φ slice around the jet direction ($|\Delta\phi| \leq 1$). The jets were selected with equal transverse energy $7 \leq E_t^{cone} \leq 8$GeV and pseudorapidity $0 \leq \eta \leq 1$ to avoid any bias coming from the position in the detector or jet narrowing effects due to large jet energy intervals. These jet profiles are shown for two bins of the parton momentum fraction of the photon $x_\gamma \geq 0.4$ and $x_\gamma \leq 0.3$ (see formula 1). Three effects are observed:

- in the photon direction ($\eta \leq 0$) low x_γ data show an enhanced energy flow wrt. the high x_γ data. This can be assigned to the remnant particles of the photon which should be reduced at high x_γ, respectively absent in the case of direct photon processes.
- In the direction of the outgoing proton ($\eta \geq 0$) the energy flow is also enhanced in the low x_γ distribution wrt. the high x_γ data. This increased energy flow indicates additional event activity for events with small parton momenta respectively large photon remnant energies.
- The jet core is narrower in the case of the high x_γ sample compared to the low x_γ sample. This effect is connected to the energy flow around the jet and the jet energy interval: since we require the jet to have $\int_{-1}^{1} E_t d\Delta\eta \sim 7$GeV a reduced energy flow around the jet enforces more energy in the core.

The energy flow of the photon remnant ($\eta \leq 0$) is well reproduced by Pythia (fig.10b). The x_γ dependent energy flow in the direction of the proton remnant ($\eta \geq 0$) is reproduced by Pythia only if it includes additional interactions between the two remnants of the photon and the proton, so called *multiple interactions*.

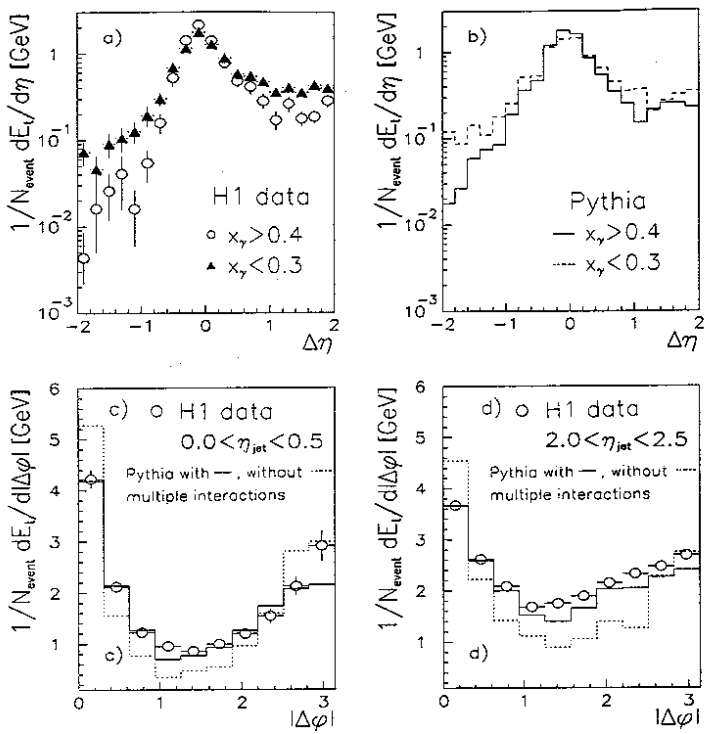

Figure 10: Transverse energy flow around the jet axis for jets with cone size $R = 1$ and transverse energy $7 \leq E_t^{cone} \leq 8$GeV. For the rapidity projection ($|\Delta\phi| \leq 1$) the jet axis is in the range $0 \leq \eta \leq 1$ and x_γ has been varied: a) H1 data for large $x_\gamma \geq 0.4$ (open circles) and small $x_\gamma \leq 0.3$ (filled triangles), b) Pythia with multiple interaction for large x_γ (full) and small x_γ (dashed). The projection on the azimuthal angle ($|\Delta\eta| \leq 1$) is shown for two bins of the jet rapidity: cd) H1 data (circles) and Pythia with (full) and without (dotted) multiple interaction.

In fig.10c,d also the transverse energy flow in the azimuthal angle Φ around the jet axis are shown in a slice of $|\Delta\eta| \leq 1$ in two bins of the jet rapidities for jets with $7 \leq E_t^{cone} \leq 8$GeV. The energy flow around the jet (*jet pedestal*) is much higher at large jet rapidities compared to the central region.

The Monte Carlo model without additional interactions (dashed line in fig.10c,d) gives no acceptable description of the jet profiles. The model with multiple interactions provides a reasonable description of the jet profile in the rapidity range $0 \leq \eta^{cone} \leq 0.5$ and shows only a

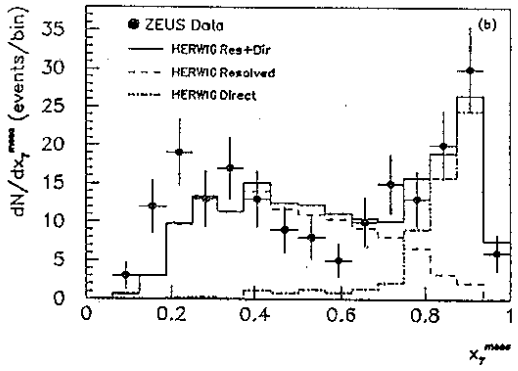

Figure 11: Signal from the LO direct photon processes at $x_\gamma^{meas} \approx 0.9$ from 2-jet data (ZEUS).

small deviation from the data at large jet rapidities $2 \leq \eta^{cone} \leq 2.5$.

The additional energy flow underneath the jets beyond what is produced by QCD radiation (fig.10cd: dotted line) is rather naturally explained by the multiple interactions picture. However, the improved description of the observed energy flow by this model is not considered as a proof of the existence of multiple interactions. Therefore a model dependence is left when the Pythia version with multiple interactions is used to extract from the observed jet spectra direct information on the underlying (LO) parton-parton scattering processes.

The comparisons of jet data to NLO calculations turn out to be much more tricky: the calculations are available only in form of jet cross sections produced on parton level. No NLO monte carlo generator exists which includes fragmentation and allows for a setup of observed-jet to parton-jet correlations. Possibilities to overcome this difficulty are being tried, but a clear recommendation for the comparison is still to be developed.

10 Direct processes

The resolved photon processes produce most of the observed jet events [22, 23]. Once this was established, the experiments searched for evidence for the direct processes. In fig.11 the distribution of the momentum fraction x_γ of partons from the photon is shown for events with two jets in the final state with more than $E_t \geq 5$GeV transverse energy per jet (ZEUS [24]). The energy of the photon E_γ in (1) has been determined from the final state hadrons.

In the same figure the prediction of the Herwig monte carlo generator is shown. The Herwig resolved processes fall towards large x_γ: with this component alone the peak observed in data at $x_\gamma \approx 0.9$ can not be explained. Only the inclusion of the Herwig direct processes gives a fair description of the large x_γ data which we take as evidence for the existence of the (LO) direct process.

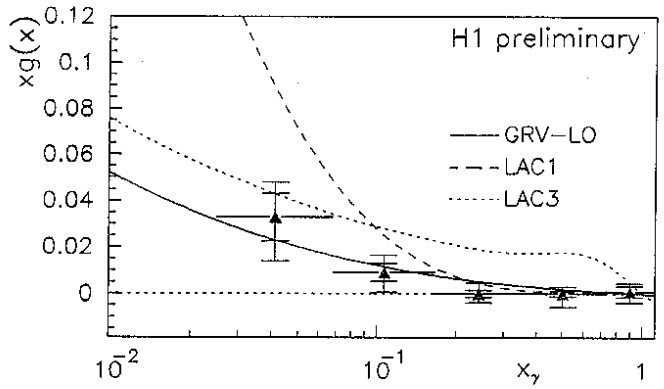

Figure 12: LO Gluon distribution of the photon from 2-jet data (H1) compared to the parametrizations of GRV (full), LAC1 (dashed) and LAC3 (upper dotted).

11 Partons in the photon

At HERA the partons of the proton probe the gluons and the quarks of the photon. To receive information on the parton momentum distributions, formula (1) was used to reconstruct x_γ^{meas} in events with two jets above $E_t \geq 7$GeV per jet. The scattered electron was required to be found in the electron tagger in order to precisely determine the energy of the photon.

The x_γ^{meas} distribution was then corrected by an unfolding method [25] to the true value of the parton momentum x_γ. The jet-parton correlations of the Pythia QCD generator with multiple interactions were used. For the photon and proton structure functions the GRV-LO parametrizations [26, 27] were chosen. The QCD scale was set to the transverse momentum generated in the parton-parton scattering process: $\mu = \hat{p}_t$. Since data and model deviate in the jet profiles (fig.10d), the transverse energies of the data jets were reduced according to the difference in the jet pedestal.

From the photon side three processes contribute: gluon, quark, and direct processes. Two of them are predicted: the resolved events with quarks from the photon by using the γ structure function F_2^γ measured in two-photon experiments and the direct processes from QCD calculations. The gluon distribution of the photon is left as the unknown and can therefore be extracted to leading order from the corrected x_γ spectrum of the 2-jet events (fig.12). The scale corresponds to $\hat{p}_t^2 \sim 60\text{GeV}^2$. This is the first measure of the gluon distribution of the photon over a large range in x_γ showing that it is small at large x_γ and exhibits a clear rise towards small parton momenta.

In the same figure, the GRV-LO [27] and LAC-1/3 [28] gluon parametrizations of the photon are compared with the data. The LAC-3 parametrization overestimates the gluon content at high

x_γ. The LAC-1 parametrization rises steeper at low x_γ than the data. The GRV-LO distribution is consistent with the measurement. In this model the gluon distribution in the photon is proportional to a meson valence quark distribution at the very low QCD scale $\mu^2 = 0.25\text{GeV}^2$. At larger scales the parton distributions are determined by the QCD evolution equations. It is interesting to note that a similar concept was used to predict the rise of the proton structure function at very small parton momenta x_{Bj}.

12 Hard scattering in events with a large rapidity gap

Rapidity gaps are regions of size $\Delta\eta \geq 1$ or more which are nearly free of any energy deposit. Many ep events show a rapidity gap between the electron and the first hadron due to the fact that the mediating photon is colour neutral. In addition to these events with electro-weak gaps events exist which have a rapidity gap from strong interactions on the proton side. They are expected for the elastic and γ-diffractive scattering processes for which the energy momentum exchange is due to a colourless state. This class of events has a large cross section and is characterized by the following criteria:

- the first energy deposit $E_t \geq E_{to}$ is visible at a rapidity η_{max} significantly smaller than the maximum rapidity which is covered by the detector thus showing a large energy free region - the rapidity gap - in the direction of the outgoing proton. Here E_{to} typically is 0.4GeV and η_{max} has to be below $1.5 - 2$ (fig.13).
- The cross section measured in terms of the rapidity gap size falls off steeply for small gaps and then flattens for large gaps before it disappears at the kinematic limit.

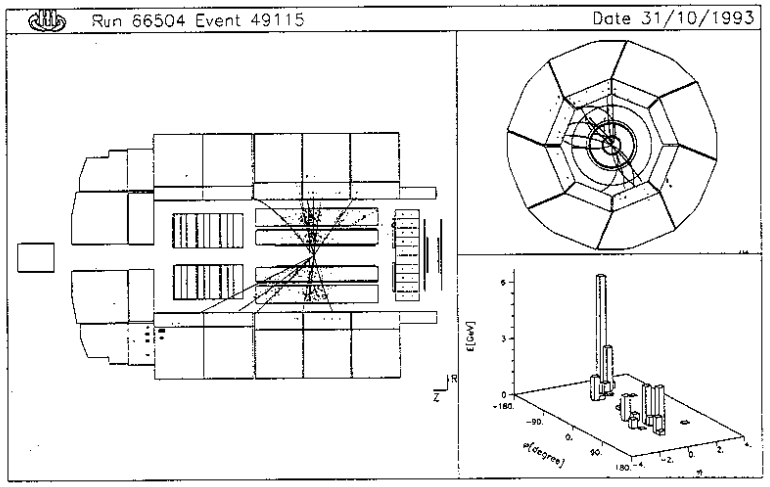

Figure 13: H1 Event with rapidity gap in the outgoing proton direction (left) and 2 jets.

A new observation boosts the interest in these events:

- a small subsample of diffractive events shows the signatures of a hard scattering processes: particles with large transverse momenta and the production of jets. The event shown in fig.13 exhibits two such distinct jets.

Jet events with rapidity gap wrt. the proton have been found in $\bar{p}p$ scattering by the UA8 experiment [29]. These events were interpreted in terms of hard Pomeron interactions: the rapidity gap is produced by the colourless Pomeron. The Pomeron consists in this picture of partons which scatter off partons from the antiproton. The hard parton-parton interactions can be calculated in QCD and challenge the experiments to determine parton distributions for the Pomeron.

It is suggestive to translate the interpretation of the $\bar{p}p$ data to the hard scattering observed in rapdity gap events of γp interactions. First studies show that this picture is indeed compatible with the photoproduction data, and different parametrizations for the Pomeron parton distributions can be distinguished.

13 Conclusions

The photon is an amazing particle:

- in one view it is a complicated object and scatters like a hadron, as can be seen from the energy dependence of the total cross section, and the relative contributions of elastic-diffractive and non-diffractive processes.
- In the other view the photon is a gauge boson which couples pointlike to quarks and leptons which is the natural interpretation of the 'direct peak' in 2-jet events, of the shape of F_2^γ (anomalous), and of the shape of the charged particle differential cross section.
- The gluon content of the photon is finally constraint. It excludes speculations about very large gluon contributions for parton momenta in the range $0.03 \leq x_\gamma \leq 1$ at the scale $\hat{p_t}^2 \sim 60\text{GeV}^2$.

The open questions to the studies at HERA on the quasi-real photon include

- the photon's behaviour in the transition region between photoproduction and deep inelastic scattering,
- a precision measurement of the Pomeron structure, and
- comparisons of the data with the NLO QCD calculations: they are needed for precise conclusions on the photon. Comparisons of jet cross sections turn out to be a challenge for theorists and experimentalists regarding the energy flow underlying the observed jets.

Acknowledgements

I wish to thank G.Jarlskog and L.Jönsson for organizing this very fruitful workshop, and F.Eisele and B.Burow for helpful advice and reading of the manuscript.

References

[1] J.J.Sakurai, Ann.Phys.11 (1960) 1

[2] T.H. Bauer, et al., Rev.Mod.Phys.50 (1978) 261, Rev.Mod.Phys.51 (1979) 407

[3] G. Schuler and T. Sjöstrand, Nucl.Phys.B407 (1993) 539

[4] M. Drees and K. Grassie, Z.Phys.C28:(1985) 451

[5] D.J. Miller, contribution to this workshop

[6] Ch. Berger and W. Wagner, Phys.Rep.146 (1987) 1

[7] AMY Collab., R.Tanaka, et al., Phys. Lett. B277 (1992) 215

[8] M. Drees, R. Godbole, Pramana J. Phys. 41 (1993) 83 and BU-TH-92-5, Dec 1992

[9] V. Barger and R. Phillips, *Collider physics*, Frontiers in physics 71, Addison-Wesley (1987)

[10] H1 Collab., I. Abt et al., *The H1 detector at HERA*, DESY preprint 93-103 (1993) 194pp

[11] Zeus Collab., *The ZEUS detector: Status report 1993*, Zeus-status-rept-1993 (1993) 597pp

[12] ZEUS Collab., M. Derrick, et al., Phys.Lett.B293 (1992) 465,
ZEUS Collab., M. Derrick, et al., DESY-94-032, Mar 1994

[13] H1 Collab., T. Ahmed, et al., Phys.Lett.B299 (1993) 374

[14] A. Donnachie, P.V. Landshoff, Phys.Lett.B296 (1992) 227

[15] E. Gotsman, talk given at the *Mini-school on low and high Q^2 diffraction at HERA*, May 4-7 1994

[16] H1 Collab., I. Abt, et al., Phys.Lett.B328 (1994) 176

[17] UA1 Collab., C. Albajar, et al., Nucl.Phys.B335 (1990) 261

[18] OMEGA Photon Collab., R.J. Apsimon, et al., Z.Phys.C43 (1989) 63

[19] J. E. Huth et al., Fermilab-Conf-90/249-E (1990)

[20] G. Marchesini, B.R. Webber, et al., Comput. Phys. Commun. 67 (1992) 465

[21] T. Sjöstrand, CERN-TH-6488 (1992)

[22] H1 Collab., T. Ahmed, et al., Phys.Lett.B297 1992) 205

[23] ZEUS Collab., M. Derrick, et al., Phys.Lett.B297 (1992) 404

[24] ZEUS Collab., M. Derrick, et al., Phys.Lett.B322 (1994) 287

[25] V. Blobel, DESY 84-118, and Proceedings of the 1984 CERN School of Computing, Aiguablava (Spain), CERN (1985)

[26] M. Glück, E. Reya and A. Vogt, Z. Phys. C53 (1992) 127

[27] M. Glück, E. Reya and A. Vogt, Z. Phys. C53 (1992) 651

[28] H. Abramowicz, K. Charchula, A. Levy, Phys.Lett.B269 (1991) 458

[29] UA8 Collab., A. Brandt, et al., Phys.Lett.B297 (1992) 417

Results from the ZEUS and H1 Experiments at HERA on the Total Photoproduction Cross Section and its Contributions

Burkhard Burow
Hamburg University, II. Institute of Exp. Physics, Hamburg, Federal Republic of Germany

This is a short overview of the photon-proton (γp) cross section measurements performed by the H1[1][2] and the ZEUS[3][4] collaborations using data from the 1992 running period of the HERA 26.7 GeV × 820 GeV electron-proton (ep) collider. A brief description of the luminosity determination is included. The interpretation of ep collisions as γp collisions is introduced and γp interactions are outlined. The total γp cross section as well as its elastic-diffractive, inelastic-diffractive and non-diffractive contributions are measured at a γp center of mass energy close to $W_{\gamma p}$ = 200 GeV; an order of magnitude higher than the energies of previous experiments. Some preliminary results, from the 1993 HERA running period, are presented for elastic γp interactions with $50 < W_{\gamma p} < 100$ GeV; where the Lorentz boost of the hadronic system allows these events to be well measured in the H1 and ZEUS detectors.

1 Introduction

The vast majority of ep interactions occur via the exchange of a virtual photon between the electron and the proton. Purely electromagnetic interactions, such as ep bremsstrahlung described below, produce only leptons and/or photons and are very accurately described by the theory of quantum electrodynamics (QED). Strong interactions, producing hadrons, are in principle completely described by the theory of quantum chromodynamics (QCD). Unfortunately, QCD can at present only be solved perturbatively, restricting its application to interactions with a large momentum transfer between the interacting particles. For example, QED and QCD can be combined to describe many aspects of deep inelastic ep scattering, where the exchanged highly virtual photon carries a large momentum and acts mainly as a point-like probe of the quark content of the proton. In contrast, hadronic γp interactions, involving a real photon or an exchanged photon of low virtuality, are dominantly soft with low momentum transfers and are thus not completely calculable by perturbative QCD. Instead, models provide a concise description of γp measurements. The measurements presented below, the first of many expected from HERA, provide constraints, beyond those of previous experiments, on γp models and should help eventually lead to a complete and presumably QCD-based theory of hadronic γp interactions.

The contribution by M. Erdmann to this conference includes an introduction and further references to the HERA accelerator, the H1 and ZEUS experiments and to ep and γp processes and kinematics.

2 The Luminosity Measurement at HERA

The luminosity (L) is determined by a count of events due to the Bethe-Heitler bremsstrahlung process, $ep \rightarrow e\gamma p$ shown in Figure 2-1, which has a large and well-understood cross section. $L = R_{ep}^{acc} / \sigma_{ep}^{acc}$, where the rate R_{ep}^{acc} of observed ep bremsstrahlung photons corresponds to the calculable cross section σ_{ep}^{acc} for the bremsstrahlung reaction corrected for the experimental acceptance and resolution.

In bremsstrahlung, the exchanged photon q carries negligible energy and momentum. The proton, incoming (p) and outgoing (p'), is essentially unaffected in the reaction. The energy of the incoming

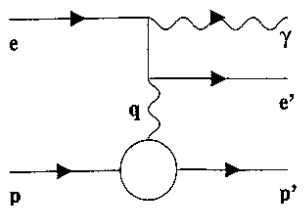

The cross section dependence on the photon exit angle is

$$\frac{d\sigma}{d\vartheta_\gamma} \sim \vartheta_\gamma \left((m_e/E_e)^2 + \vartheta_\gamma^2 \right)^{-2},$$

which peaks near $\vartheta_\gamma \sim m_e/E_e \sim 0.02$ mrad ~ 2 mm / 100 m.

The electron scatter is of order $\vartheta_{e'} \sim m_e/E_{e'}$.

Figure 2-1 The Bethe-Heitler Bremsstrahlung Process.

electron (e) is effectively shared by the outgoing electron (e') and photon (γ), $E_e = E_{e'} + E_\gamma$. At the design luminosity of order 10^{31} cm^{-2} s^{-1}, HERA produces a 1 MHz rate of events with $E_\gamma > 5$ GeV; demonstrating the potential for a negligible statistical error in the luminosity determination.

As described in Figure 2-1, the exit angles of the outgoing electron ($\vartheta_{e'}$) and the outgoing photon (ϑ_γ) are negligible with respect to the incoming electron and hence to the HERA electron beam. The photon scattering angle of approximately 0.02 mrad is smaller than the angular spread of order 0.1 mrad of the electron beam at the interaction point (IP). Therefore, the outgoing electron and photon are measured by detectors integrated with the HERA beamline, as shown in Figure 2-2 a). Electrons scattered within a very small angle of approximately $\vartheta_{e'} < 6$ mrad and with a fraction of the electron beam energy, approximately $0.2 < E_{e'}/E_e < 0.9$, are deflected by the bending magnets out of the outgoing electron beam pipe and into the electron calorimeter of the luminosity monitor. Photons produced in the electron beam direction remain in the proton beam pipe until the pipe and the proton beam bend, at which point the photons exit the pipe and enter the photon calorimeter. The agreement of the measured and simulated photon energy spectrum shown in Figure 2-2 b) demonstrates that the performance of the luminosity monitor is well understood.

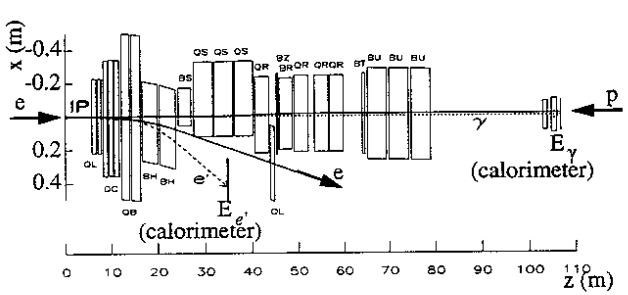

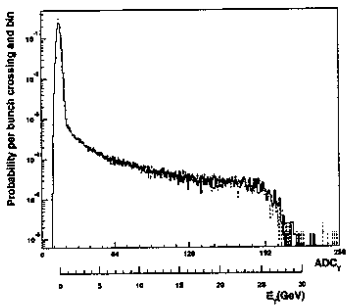

Figure 2-2 The Luminosity Monitor.

a) *The x and y axes have different scales. The HERA e- and p-beams meet at the interaction point (IP) and are focussed or bent by the magnets labelled Q and B. Of the ZEUS or equivalently H1 detector, only the electron and photon calorimeters are shown along with the HERA magnets.*

b) *Measured (dashed error bars) and simulated (solid line) bremsstrahlung photon spectrum at ZEUS.*

A background of order 30 % to ep bremsstrahlung, with the same experimental signature, is $eA \rightarrow e\gamma A$ bremsstrahlung involving the HERA electrons and the residual gas in the beamline. An electron pilot bunch, not paired to a proton bunch, provides a measurable eA bremsstrahlung rate (R_{pilot}). The ratio of the electron currents for the pilot (I_{pilot}^e) and all (I_{tot}^e) bunches permits the statistical removal of the eA bremsstrahlung rate from the total bremsstrahlung rate (R_{tot}), with $R_{ep}^{acc} = R_{tot} - R_{pilot} \cdot I_{tot}^e / I_{pilot}^e$.

The H1 luminosity determination required the observation of both the electron and the photon for the counted bremsstrahlung events using the energy constraint $E_{e'} + E_\gamma = E_e$ within experimental resolution. Since there was negligible non-bremsstrahlung background in the photon calorimeter, the ZEUS determination simply counted events with $E_\gamma > 5$ GeV and ignored the bremsstrahlung electron. Systematic errors of the luminosity determination are presented in Table 2-1.

Error [%]	Bethe-Heitler	Acceptance	Calibration, Resolution	eA Subtraction	Multiple Events	Event Count	Electron Satellite	Total
H1	0.3	5.5	2.0	2.0	-	2.5	-	7.0
ZEUS	1.0	2.0	2.5	2.0	1.0	0.5	1.5	4.3

Table 2-1 Systematic Errors in 1992 Luminosity Determination

3 Photon-Proton Interactions at the Electron-Proton Collider HERA

In an ep collision which scatters the electron by only a small angle ϑ, the exchanged photon (γ) is only slightly virtual. The kinematic variables are given to excellent approximation by

$$E_\gamma \approx E_e - E_{e'}, \quad y \approx E_\gamma / E_e, \quad Q^2 - Q^2_{\min} \approx E_e E_{e'} \vartheta^2, \quad Q^2_{\min} = m_e^2 y^2/(1-y), \quad W_{\gamma p} \approx 2\sqrt{E_\gamma E_p}. \quad (3\text{-}1)$$

The ep interaction may be conceptually broken down into two parts, $ep \rightarrow e' + \gamma p$ and $\gamma p \rightarrow H$. In the first, the electron is considered to be accompanied by a flux of virtual photons. At low virtualities, the exchanged γ can be shown to behave like a real photon, thus the second part is true photoproduction[5].

Pragmatism provides two classes of photoproduction at ZEUS and H1. Tagged photoproduction refers to events whose scattered electron escapes down the beam pipe and enters the electron calorimeter of the luminosity monitor, thus providing an accurate measurement of the photon in collision with the proton. The aperture of the HERA beamline restricts the tagged events to approximately $Q^2 < 0.02$ GeV^2 and $130 < W_{\gamma p} < 260$ GeV. Untagged photoproduction refers to events whose scattered electron simply escapes the central detector down the beam pipe. The incoming photon can only be reconstructed from measurements on the produced hadronic system. With a hole in the central detector of approximately 3° for the beam pipe, these untagged events have a photon virtuality restricted to approximately $Q^2 < 4$ GeV^2. Events from the complete γp center of mass energy range, $m_p < W_{\gamma p} < \sqrt{s_{ep}} = 296$ GeV, are available for measurement.

The tagged events suggest measuring $\sigma^{\gamma p}_{\text{tot}}$ by simply counting the scattered electrons and determining the electron tagging efficiency. Thus, the complicated hadronic product, not yet well understood at HERA energies, could be ignored. Alas, electromagnetic interactions make this measurement difficult, if not impossible. Bremsstrahlung electrons and other electromagnetic interactions, such as electron-positron pair production, provide huge backgrounds. Large radiative corrections are also associated with such a measurement. Therefore, the $\sigma^{\gamma p}_{\text{tot}}$ measurement requires the observation of the produced hadronic system.

Photoproduction is usually expressed in terms of the vector meson dominance (VMD) model. The photon and the vector mesons ($V = \rho, \omega, \phi, \ldots$) have identical quantum numbers, allowing the photon to couple to a vector meson which then interacts with the proton. The interaction produces a final hadronic state very similar to that of hadron-hadron (e.g. πp) collisions. Thus the reaction is either elastic-diffraction ($\gamma p \rightarrow Vp$), single-diffraction of the proton ($\gamma p \rightarrow VX_p$), single-diffraction of the photon ($\gamma p \rightarrow X_V p$), double-diffraction ($\gamma p \rightarrow X_V X_p$) or non-diffraction ($\gamma p \rightarrow X$). Previous γp measurements were restricted to $W_{\gamma p} < 18$ GeV. Therefore, the characteristics and relative frequency of each component are not known a priori at HERA energies.

Due to the momentum imbalance in the collision of the 820 GeV proton and the < 26.7 GeV photon, the γp product at HERA has a large Lorentz boost in the ZEUS and H1 detectors. As demonstrated in Figure 3-2, the effect of the boost is conveniently examined in terms of the rapidity, $y_{\text{rapidity}} \equiv \frac{1}{2}\ln(E+p_z/E-p_z)$, of the outgoing particles. Under a boost β, the rapidity approximately changes as $y_{\text{rapidity}} \rightarrow y_{\text{rapidity}} + \tanh^{-1}\beta$. For a typical tagged photoproduction event with $E_\gamma = 10$ GeV, Figure 3-2 demonstrates that many of the decay particles of the elastically produced vector mesons escape the central detector down the beampipe. Lower photon energies correspond to a larger $\tanh^{-1}\beta$. Therefore, for a range of lower photon energies, corresponding roughly to $10 < W_{\gamma p} < 100$ GeV, the decay products of the elastic vector mesons have little boost and may be measured in the central detector.

Figure 3-1 The Rapidity Distribution of the Final Hadronic State Particles.
The boundaries of the forward (FCAL, proton direction), barrel (BCAL), and rear (RCAL) calorimeters of the ZEUS central detector are shown. Arbitrary normalizations apply to the simulated qualitative rapidity distributions of particles from γp collisions from a 10 GeV *tagged photon. The decay products of the vector mesons produced in elastic-diffraction ($\gamma p \rightarrow Vp$, dashed line) are accepted by RCAL or escape down its beam pipe. The lightly scattered proton escapes down the FCAL beampipe.*
For double-diffraction ($\gamma p \rightarrow X_V X_p$, dotted line), the particles from the diffracted photon enter mainly RCAL and BCAL. Most particles from the diffracted proton escape down the FCAL beam pipe, with some observed in FCAL.
The particles of non-diffractive events (solid line) are observed everywhere in CAL, but mainly in FCAL. The distribution peaks for transverse particles in the γp center of mass system, corresponding to $y_{\text{rapidity}} \approx 2.2$.

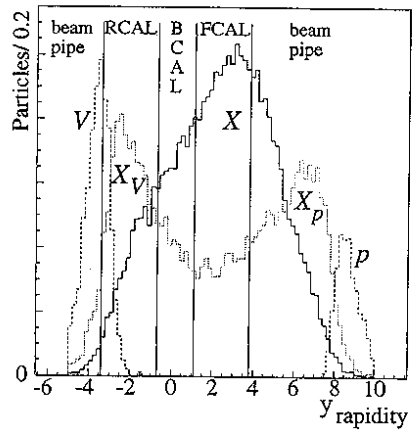

4 Photon-Proton Cross Section Measurements at HERA

The requirements for the events counted for the determination of $\sigma^{\gamma p}_{\text{tot}}$ are given in Table 4-1. The electron tag accurately measures E_γ and hence $W_{\gamma p}$. The tag also allows for a closer examination of the energy dependent hadronic system and its acceptance in the central detector. The hadronic acceptance depends in part on E_γ due to the varying Lorentz boost of the γp system. Since the scattered electron is described by QED, the systematic error of the electron acceptance given in Table 4-1 reflects the uncertainty surrounding the electron arm of the luminosity monitor. The systematic error associated with the H1 electron acceptance is only half as large as that for ZEUS. Due to the narrow electron energy window for the ZEUS measurement, the acceptance is more sensitive to the exact energy scale calibration of the electron calorimeter. In addition, some of the systematic errors of the H1 electron acceptance determination cancel with those of the H1 luminosity determination, since the latter measures the bremsstrahlung electron.

Requirement	H1	acceptance	ZEUS	acceptance
hadronic system in central detector	≥ 1 track from IP	57±5 %	$E_{\text{RCAL}} > 0.7$ GeV	76±5 %
tag of scattered electron	$5 < E_{e'} < 22$ GeV	35±2 %	$15.2 < E_{e'} < 18.2$ GeV	77±7 %

Table 4-1 Requirements on Events for the Total Photoproduction Cross Section Determination
Further analysis treats background and radiative events, with a small contribution to the systematic error.

The systematic error for the acceptance of the hadronic system is dominated by the uncertainty for γp physics at HERA. The range of possible γp behavior is taken from extrapolations of hadron-hadron and low energy γp measurements and is input to Monte Carlo simulations. The accepted simulated events are required to be consistent with the characteristics measured for the hadronic system in the central detector.

The acceptance of the hadronic system by the 1992 H1 trigger is of order 90 % for hard and 60 % for soft non-diffractive processes, 50 % for photon-diffractive processes ($\gamma p \rightarrow X_V p$ or $X_V X_p$) and 0 % for photon-elastic processes ($\gamma p \rightarrow Vp$ or VX_p), with errors due to the range of event characteristics possible for the individual processes. The characteristics, as yet unmeasured at HERA energies, include the transverse momentum distributions for diffraction and for the primary hadrons in the fragmentation of hard processes. Nevertheless, the dominant systematic error of the acceptance is due to the uncertainty for the fraction of photoproduction due to the individual processes. These fractions have not yet been determined by H1, but the simulation best describes the data with $\sigma_{diffr.}/\sigma_{tot} = 0.26\pm0.06$, $\sigma_{soft}/\sigma_{tot} = 0.55\pm0.15$ and $\sigma_{hard}/\sigma_{tot} = 0.19\pm0.15$, where the errors are a conservative estimate of the uncertainty in the composition. The inclusive particle transverse momentum distribution and the polar angle distribution are among those distributions compared between the data and the simulation.

The resulting H1 measurement, at $\langle W_{\gamma p} \rangle = 197$ GeV, is $\sigma_{tot}^{\gamma p} = 156\pm2\pm18$ μb [2].

The ZEUS determination of the hadronic acceptance also faces the above uncertainties for photoproduction at HERA, but has two advantages over the H1 determination. Firstly, the acceptance of the hadronic system varies less across processes for ZEUS than for H1. The acceptance of the 1992 ZEUS trigger is of order 90 % for non-diffractive processes, 60 % for inelastic-diffraction and 30 % for elastic-diffraction. Secondly, the acceptance studies of ZEUS measure the individual contributions due to the elastic-, inelastic- and non-diffractive processes. The processes are distinguished by their measured energy distributions in the calorimeter (CAL) of the ZEUS central detector. The ZEUS determination is simplified by choosing tagged electrons for an essentially monochromatic photon beam with $E_\gamma = 10$ GeV.

For the ZEUS event sample, only diffractive events have no energy observed in the proton direction; $E_{FCAL} < 1$ GeV for the forward calorimeter. As already demonstrated in Figure 3-2, the decay particles of the elastically scattered vector mesons remain closer to the rear, electron direction, beampipe than the particles of an inelastic scattering. A quantitative difference between elastic and inelastic simulated events is shown in FIGURE 4-1 a), using the measured energy weighted radius in the rear calorimeter, $R_{RCAL} \equiv \sum rE / \sum E$. Due to the reconstruction procedure, the radius r may lie inside the beampipe. As shown in Figure 4-1 b), the proportion of each process can be determined by combining the two simulated distributions such that the sum best fits the measured data.

Events in the ZEUS sample with energy in the forward direction, $E_{FCAL} > 1$ GeV, are dominantly non-diffractive. The characteristics of the γp simulations are constrained by a simultaneous fit to the measured energy distribution in the forward (E_{FCAL}) and in the central (barrel, E_{BCAL}) regions. Systematic errors in the hadronic acceptance are estimated by examining three types of non-diffractive γp simulations: hard processes (mini-jets of PYTHIA or HERWIG) plus soft processes (PYTHIA 2-string model), phenomenological QCD (PYTHIA minimum bias), $p\bar{p}$ parametrization (HERWIG minimum bias). The best fit to the data for the latter two simulations is shown in Figure 4-1 c).

In addition to the information from the above energy distributions, the ZEUS γp analysis uses one extrapolation of inelastic-diffractive behavior determined at low energies, $\sigma_{VX_p} = \sigma_{X_V p} = 2\sigma_{X_V X_p}$, when either the proton, the meson or both particles diffractively dissociate in the scattering. The resulting ZEUS measurement, at $\langle W_{\gamma p} \rangle = 180$ GeV, is $\sigma_{tot}^{\gamma p} = 143\pm4\pm17$ μb with 64±4 % due to non-diffractive processes, 23±5 % due to inelastic-diffraction and 13±5 % due to elastic-diffraction[3].

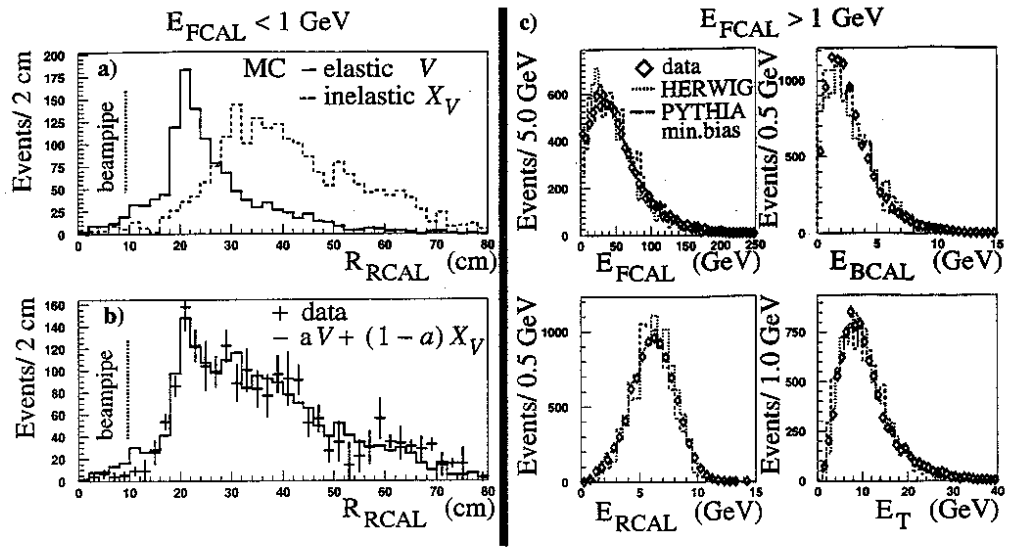

Figure 4-1 Energy Distributions for Photoproduction at ZEUS with $E_\gamma = 10$ GeV.

5 Elastic Vector Meson Production at HERA

At HERA, elastic-diffractive events, $ep \rightarrow eVp$, with approximately $10 < W_{\gamma p} < 100$ GeV, produce vector mesons with little Lorentz boost, allowing the decay particles to be well measured in the H1 and ZEUS central detectors. Both the electron and the proton escape undetected down the beampipe, but much of the kinematics may be reconstructed just from the vector meson decay particles. Preliminary results by H1, based on the 1992 run period, were shown in [2].

In 1993, ZEUS collected a sample of 10^4 elastically produced rho mesons, which decay almost exclusively as $\rho^0 \rightarrow \pi^+\pi^-$. A candidate event is shown in Figure 5-1 a). The trigger required a 0.5 GeV electromagnetic energy deposit in RCAL, which restricts the $W_{\gamma p}$ acceptance but allows backgrounds to be strongly suppressed. The event selection includes requirements for exactly two oppositely charged tracks which come from the interaction point and which match with the energy deposits in the calorimeter. The resulting acceptance is approximately 9 % for $50 < W_{\gamma p} < 100$ GeV, $0.5 < m_{\pi\pi} < 1.0$ GeV in the two pion system and $p_T^2 < 0.5$ GeV^2 for the transverse momentum transfer between the meson and the proton.

A preliminary acceptance corrected ρ mass peak is shown in Figure 5-1 b). The mass and width resulting from the fit, $m_\rho = 762\pm10$ MeV and $\Gamma_\rho = 169\pm14$ MeV, agree with expectations. In addition to the elastic ρ, the 1993 data includes clear signals for the other elastically produced vector mesons, including the decay channels $\omega \rightarrow \pi^+\pi^-\pi^0$, $\phi \rightarrow K^+K^-$ and $J/\psi \rightarrow e^+e^-$ or $\mu^+\mu^-$.

For $\gamma p \rightarrow Vp$ analysis at HERA, a major difficulty is the indistinguishable inelastic background $\gamma p \rightarrow VX_p$, since the low mass X_p usually escapes the central detector down the proton beam pipe. For the 1994 data onwards, ZEUS and H1 should be able to conclusively resolve this issue using newly commissioned hardware in the proton direction, including the leading proton spectrometer of each experiment.

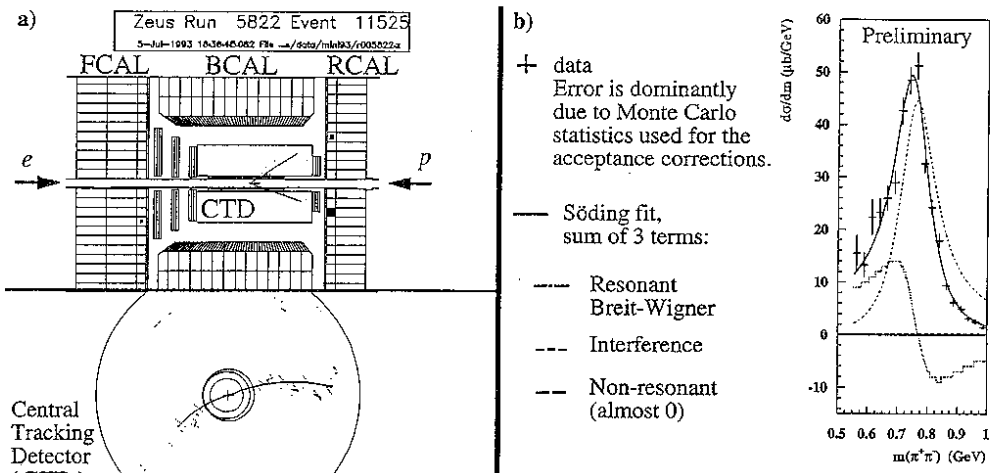

Figure 5-1 Elastically produced rho mesons at ZEUS.

6 Results

The energy dependence of $\sigma_{tot}^{\gamma p}$ is displayed in Figure 6-1 a), which includes the low energy measurements of earlier experiments. The HERA measurements are in agreement with the DL and ALLM parametrizations of Regge-type analyses and with a mini-jet calculation using $p_T^{min} = 2$ GeV and the DG parametrization of the photon structure function [6]. The partial cross sections of $\sigma_{non\text{-}diffr.}^{\gamma p} = 91 \pm 11$ μb, $\sigma_{inel\text{-}diffr.}^{\gamma p} = 33 \pm 8$ μb and $\sigma_{el\text{-}diffr.}^{\gamma p} = 18 \pm 7$ μb obtained by ZEUS are consistent with the expected results of a recent phenomenological parametrization[7]. Figure 6-1 b) presents the ZEUS and low energy measurements for the elastic-diffractive cross section along with the parametrization.

These cross section measurements are among the first contributions from HERA to γp physics. ZEUS and H1 continue to exploit the unique γp laboratory offered by HERA. Future measurements will describe the final hadronic system with increasing detail and provide stringent tests for the theoretical description of photoproduction processes. Among the first of these new results will be the description of the simplest hadronic system, that of elastic vector meson scattering.

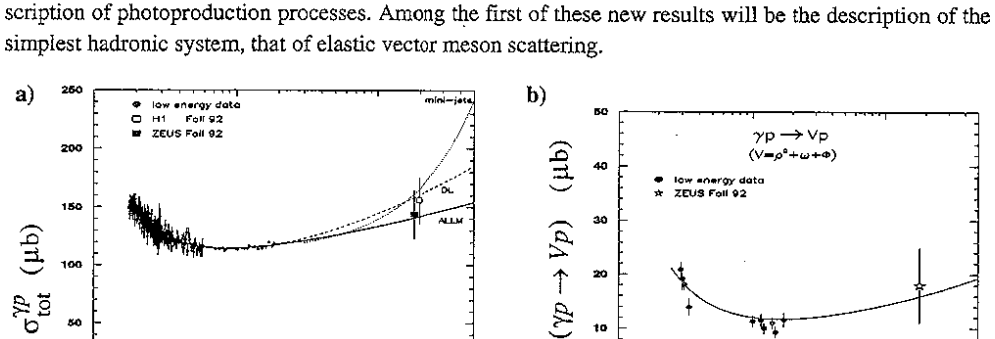

Figure 6-1 The Energy Dependence of the Total and the Elastic Photoproduction Cross Sections.

7 References

[1] H1 Collab., T. Ahmed et al., *Phys. Lett.* **B299** (1993) 469.

[2] S. Levonian, Low and Medium p_T Photoproduction at HERA, in DESY 93-077 (1993).

[3] ZEUS Collab., M. Derrick et al., DESY 94-032 (1994), to appear in *Z. Phys.* **C**.

[4] B. Burow, A Measurement of the Total Photon-Proton Cross Section in the Center of Mass Energy Range 167 to 194 GeV, Ph. D. Thesis, Graduate Department of Physics, University of Toronto, Canada (1994) available as Internal Report DESY F35D-94-01 February 1994.

[5] V. M. Budnev, I. F. Ginzburg, G. V. Meledin, V. G. Serbo, *Phys. Rep.* **15C** (1975) 181.

[6] A. Donnachie, P. V. Landshoff, *Nucl. Phys.* **B244** (1984) 322;
H. Abramowicz, E. Levin, A. Levy, U. Maor, *Phys. Lett.* **B269** (1991) 465.
M. Drees, K. Grassie, *Z. Phys.* **C28** (1985) 451.

[7] G. A. Schuler, T. Sjöstrand, *Phys. Lett.* **B300** (1993), *Nucl. Phys.* **B407** (1993) 539.

Photoproduction at HERA and the Behaviour of the Photon

L.Stanco

I.N.F.N. – Padova

Several aspects of the hard photoproduction processes at HERA are presented, with particular reference to the definition of the photon. Two major kind of results are discussed: single particle spectra and jet production. First results on heavy quark production are also presented.

1 Introduction

The photon at HERA is the most important interacting particle, considered as current or as beam itself. Actually the photoproduction processes provide most of the cross-section and open the study to a large set of reactions. The energy of the center of mass has an upper limit of 300 GeV; one order of magnitude greater than that of previous fixed target experiments. The photoproduction cross-sections are usually obtained from the full electroproduction one by unfolding the photon flux as $\sigma_{e-p} = F_\gamma \cdot \bar{\sigma}_{\gamma-p}$, where:

$$F_\gamma = \frac{\alpha}{2\pi} \cdot \int_{y_{min}}^{y_{MAX}} [\frac{1+(1-y)^2}{y} \ln \frac{Q^2_{MAX}(y)}{Q^2_{min}(y)} - \frac{2(y-1)}{y}(1 - \frac{Q^2_{min}}{Q^2_{MAX}})]dy$$

and $Q^2_{min} = \mathcal{O}(10^{-7} GeV^2)$.

The important variables in the quasi-real photon interactions are obviously the virtuality of the photon (Q^2), which at HERA is usually below few GeV^2 if the antitagging of the electron scattering in the calorimeter is requested or below 10^{-2} GeV^2 if tagged in the Luminosity detector (see B. Burrow's contribution to these proceedings). Another variable is y, related to the fraction of the energy carried by the photon with respect to the incoming electron. It corresponds to the energy of the center of mass of the $\gamma - p$ collisions in the low Q^2 limit. The total hadronic mass, W, given by the sum of all the hadronic (i.e. without the scattered electron) final states, also corresponds to the center of mass of the $\gamma - p$ system and it averages at 200 GeV ($s_{\gamma p} = y \cdot s_{ep} = W^2$, for low Q^2).

The photoproduction processes are largely important to perform QCD tests and studies of the strong interactions coupled to the photon, studies done via the structure function of the photon. Generally speaking, we are also interested in the nature of the photon itself and the unfolding of its different behaviours, as well as the correlated study of the proton structure function. In this part of the proceedings we will focus on the last two points: nature of the photon and proton structure function as can be extracted by the photon interactions.

Following [1], for example, the state function of the photon can be tried to be written as superposition of different state functions (fig. 1):

$$|\gamma> = c_{bare}|\gamma_{bare}> + \sum_{V=\rho,\omega,\phi,J/\psi} c_V|V> + \sum_{q=u,d,s,c,b} c_q|q\bar{q}> + \sum_{l=e,\mu,\tau} c_l|l^+l^->$$

The second contribution corresponds to the Vector Meson Dominance (VMD) part where the photon couples directly to the vector meson hadrons and it behaves like a normal hadron. To this respect photoproduction is equivalent to hadroproduction. The third contribution corresponds to oscillations of the γ into $q\bar{q}$ states and it may be computed perturbatively. This part is a new one present at HERA and it can be distinguished from the VMD processes by the scale k_T of the *parton* which is *extracted* from the photon (see G. Schuler's contribution to these proceedings). It's usually

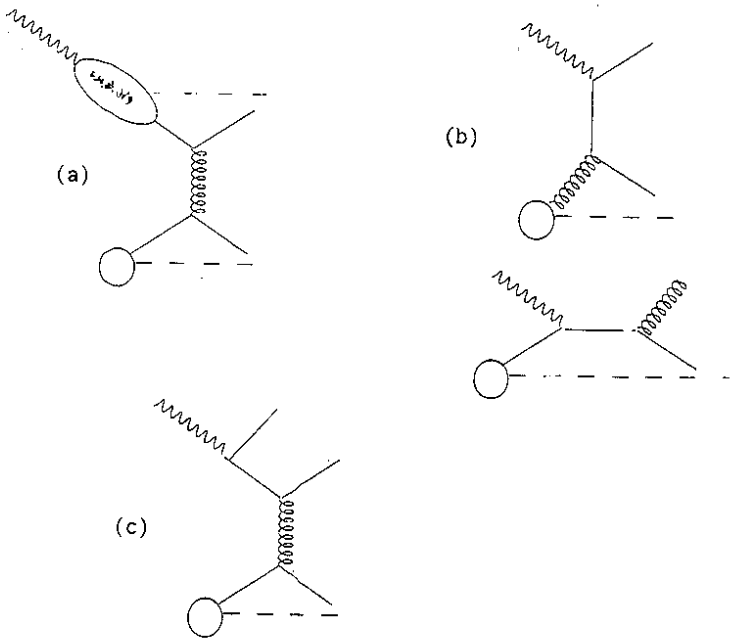

Figure 1: Hard scatterings for quasi–real photons. (*a*) VMD process, (*b*) the two direct processes: photon–gluon fusion and QCD Compton, (*c*) anomalous production. The dashed lines represent the remnants.

called the *anomalous* contribution and correspondly the *anomalous* behaviour of the photon. It can be considered as the phenomenological bridge to the higher orders of the direct photon interactions. The first contribution corresponds in fact to the direct process where the photon couples directly to the partons of the protons. It can be defined as difference from the other contributions to full photoproduction. We have discarded from the discussion the last term which describes the γ oscillations to the lepton pairs, since they do not undergo strong interactions at leading order. It is may be important to note that all the relevant processes (VMD, anomalous and direct) are of the same order of magnitude in terms of coupling constants ($\mathcal{O}(\alpha_{EM} \cdot \alpha_{Strong})$), even if strong different scales show up in the differential distributions, once for all the p_T of the final states.

Pomeron exchange constitutes an orthogonal aspect of photoproduction reactions, where *pomeron* refers to the exchange of a current with the quantum numbers of the vacuum, and usually identifies the so called diffractive processes. In this paper we are interested only in the hard non–diffractive interactions. This is equivalent to requiring the color flow of QCD between all the partons of both the initial and the final states at Born level, i.e. of the hard sub–process. The question about a possible transition between diffractive and non–diffractive components, which appears to be rather intriguing at least by a phenomenological point of view, is an important one to be addressed to the *pomeron* and *QCD–parton* exchange studies.

The experimental division between *resolved* and *direct* photon production is related to the above decomposition by merging the VMD semi–hard and the anomalous processes. An experimental distinction has not yet been provided, even if the understanding and description of the *photon remnant* jet likeness is probably a good possibility. The *resolved* part owns a major interest in the study of the photon constituents via its structure function.

The direct photon reactions are strongly related to the study of the gluon content inside the proton and the small–x behaviour, as it is also reported in the following.

The Detectors

The two detectors of HERA, H1 and ZEUS, have a similar setup, the main distinction being in the choice of the calorimeter. H1 uses a liquid argon calorimeter which

covers the angular region $4° < \theta < 153°$, with an energy resolution of $12\%/\sqrt{E} \oplus 1\%$ (E in GeV) for electron, and $50\%/\sqrt{E} \oplus 2\%$. The ZEUS calorimeter is a compensating uranium-scintillator detector, with response $e/h = 1.00 \pm 0.03$ for momenta above 3 GeV/c, and energy resolution of $18\%/\sqrt{E}$ for electron, $35\%/\sqrt{E}$ for hadron. The angular coverage of the ZEUS calorimeter corresponds to $2.6° < \theta < 176.1°$.

The tracking devices have a resolution in transverse momentum for full length tracks of $\sigma_{p_T}/p_T^{track} = 0.009 \cdot p_T^{track}(GeV/c)^{-1}) \oplus 0.015$ and $0.005 \cdot p_T^{track} \oplus 0.016$ for H1 and ZEUS, respectively.

2 Single particle spectra

Distributions of the inclusive charged particle productions have been first obtained by the H1 collaboration[2] in the 1992 data sample, and secondly by ZEUS[3] with the 1993 data sample. Both the experiments have been limited to the pseudorapidity region $|\eta| = |-\ln tg\frac{\theta}{2}| \leq 1.5$ of the charged particle while the chosen minimum p_T is of 0.3 GeV/c and 0.2 GeV/c for H1 and ZEUS, respectively. Events are tagged by the luminosity monitor, via the scattered electron. The transverse momentum of the leading charged particle in the event, $p_T^{leading}$, is an important scale to try to disentangle the soft/hard interaction ratio, as well as to extract information on several Monte Carlo variables like the p_T^{min}, the minimum transverse momentum of the outgoing parton, the relative rate of the multiple interaction considered as a general description of the soft underlying event, the different structure functions and fragmentations. In fig. 2 data from H1 are compared with two different kinds of Monte Carlo.

When compared with the different simulations of the hard and the soft interactions, events by H1 show a good agreement and suggest to follow the Monte Carlo indication that the soft component dies out towards 1.5 GeV/c of $p_T^{leading}$. The connection of the photon behaviour at small p_T with the hadron one can be tested with the $p\bar{p}$ collisions. The ZEUS result with 1993 data for a p_T less than 2 GeV/c show a general good agreement with UA1[4] data, after an overall normalization, when the

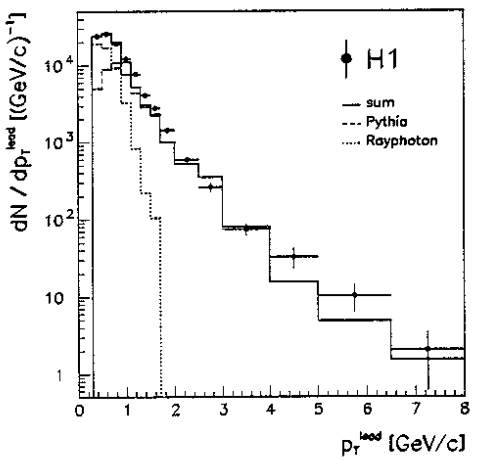

Figure 2: Measured uncorrected distribution of $p_T^{leading}$ (full circle). The histograms represent the corresponding distributions for the PYTHIA full parton shower Monte Carlo (dashed) and the RAYPHOTON soft meson–proton interaction simulation (dotted), and their sum (full).

comparison is done for the center of mass energy at 200 GeV. At higher energies of the $p\bar{p}$ center of mass (380 and 540 GeV) the inclusive $p_T^{leading}$ distribution is stiffer and follows the general trend also supported by the comparison with the ISR data at 63 GeV. The p_T distributions are however less stiffer than the corresponding ones at HERA (see fig. 3). The conclusion seems to be rather clear and it points towards an explicit hadronic "identification" of the photon at such energy scales, together with an increasing contributions of the direct and the anomalous parts. For the latter contributions some indications were also given by the OMEGA photoproduction experiment[5].

3 Jet production

Jet at HERA are mostly defined by the cone algorithm, applied to the calorimeter structure and with a cone size $R = \sqrt{\Delta\varphi^2 + \Delta\eta^2} \leq 1$. The cone algorithm defines an arbitrary number of jets per event, which depends on the energy thresholds on the single cell (seed and companions) and the total minimum energy of the jet itself. By contrast, the k_T algorithm performs a clustering by using the relative momentum and a prefixed global number of jets in the event. It may be important for studies of the remnant jet and first results from ZEUS[6] shows evidence of a remnant component when the k_T algorithm is applied: three jets are required per events and when the first 2 jets are identified by comparison with the cone reconstruction, the third one is clearly a jet in the rear direction. The rather preliminary (not conclusive) result from ZEUS is that the *remnant* jet shows no relevant difference to the other hard scattering jets (see fig. 4).

The cone algorithm has however allowed to state a large set of interesting results on the behaviour of the jets at HERA. The inclusive distribution has been used by H1 to obtain insights of the photon structure function (see R.Kaschowitz's contribution to these proceedings). Preliminary ZEUS results[7] with 1993 data sample on the inclusive η_{jet} and E_{jet}^T distributions show good agreement with Monte Carlo and possible sensitivity to different photon structure functions, expecially in the forward

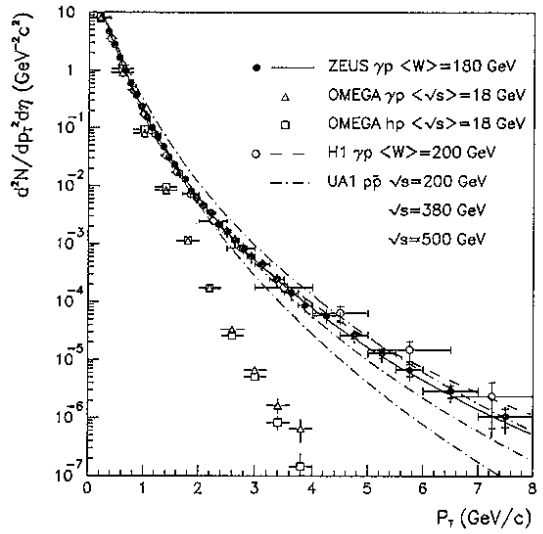

Figure 3: Comparison of transverse momentum spectra. The solid points indicate ZEUS non–diffractive data at $\langle W_{\gamma p}\rangle = 180\ GeV$, open circles – H1 data at $\langle W_{\gamma p}\rangle = 200\ GeV$, squares – OMEGA πp data at $\langle\sqrt{s}\rangle =\ GeV$, triangles – OMEGA γp data. The inner error bars indicate statistical errors and the outer ones the linear sum of statistical and systematic errors. The solid line is a power law fit to ZEUS data, dashed line to H1 data, dashed-dotted line to UA1 $p\bar{p}$ data at $\sqrt{s} = 200\ GeV$, $\sqrt{s} = 380\ GeV$ and $\sqrt{s} = 500\ GeV$. The data from other experiments have been normalized to ZEUS non–diffractive data at $p_T < 1.2\ GeV/c$.

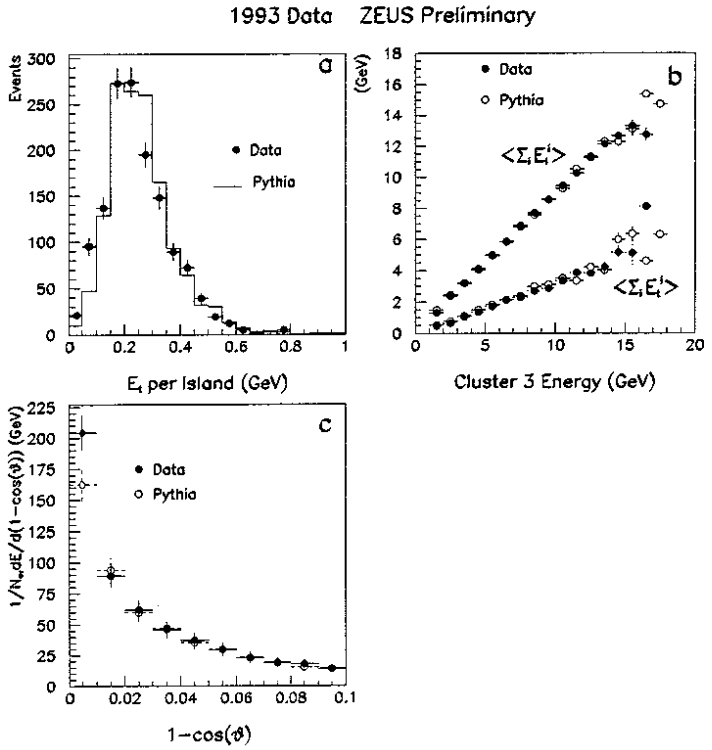

Figure 4: Jet characteristic for the cluster identified as the remnant (third jet): (a) the average transverse energy with respect to the cluster axis per single region of the calorimeter (*islands*); (b) distribution of the average energy transverse and longitudinal to the cluster axis as a function of the cluster energy itself; (c) energy flow as a function of $(1-\cos\theta)$, where θ is the angle between the cluster axis and the calorimeter cell. In (a) ZEUS data and Monte Carlo are normalized to the number of events in the data. In (b) the error bars are the errors on the mean: those points at the high energy with no error bars are the result of a single entry in that bin.

region (see figs. 5 and 6).

The photon behaviour in the hard processes can be simply established by considering the two–jet sample. In fact, the final state of the two jets can be easily connected with the fractional momenta of the two incoming partons. By naming x_γ and x_p the two fractional momenta of the partons (a and b) coming from the photon and the proton, respectively, one obtains:

$$x_\gamma = x_a = \frac{E_a}{E_\gamma} = \frac{\sum_{jets} E_i \cdot (1-\cos\theta_i)}{2 \cdot E_\gamma}$$
$$x_p = x_b = \frac{E_b}{E_p} = \frac{\sum_{jets} E_i \cdot (1+\cos\theta_i)}{2 \cdot E_p}$$

Essentially two ways are available to compute E_γ, one from the luminosity detector, and one from the Jacquet–Blondel method:

$$E_\gamma = \frac{1}{2}\sum_{cells} E_i \cdot (1-\cos\theta_i) = y_{JB} \cdot E_e$$

In the first case, small values (< 0.5) for x_γ are privileged, while the second one is optimal to make evidence of the $x_\gamma \approx 1$ region which corresponds to the direct photon processes (the parton a coincides with the incoming γ). ZEUS results from 1992 data[8] have in fact demonstrated the clear evidence for the direct process peak at around $x_\gamma \approx 1$. The 1993 data sample has confirmed with quite higher statistics this result (fig. 7).

The extraction of the parton distribution as computed at the lowest tree level has been shown to work out the disentangling of the first rough separation between hadronic and point–like behaviour of the photon. It is not yet clear which procedure will be optimal to unfold the parton distributions inside either the photon or the proton. Inclusive methods would perhaps be important to use once the number of contributing processes grows too much.

Measure of heavy flavor production will be extremely important in exploiting such studies, since their direct correlation with the gluon content in either the photon or the proton is established. Preliminary results from both H1 and ZEUS are available for the production of the J/ψ and the D^* mesons. In the case of the J/ψ, clear peaks are seen in the leptonic channels, e^+e^- and $\mu^+\mu-$, with a bunch of hundred events,

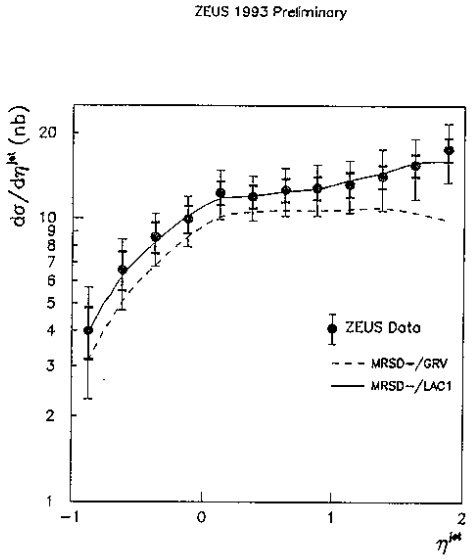

Figure 5: Measured differential cross section for inclusive jet production as a function of η_{jet} (black dots; thick error bars indicate the statistical errors of the data and MC used to calculate the corrections; thin error bars indicate the statistical and the systematic errors added in quadrature) compared to PYTHIA expectations including resolved and direct processes for two parametrizations of the photon parton distributions: GRV (dashed line) and LAC1 (solid line).

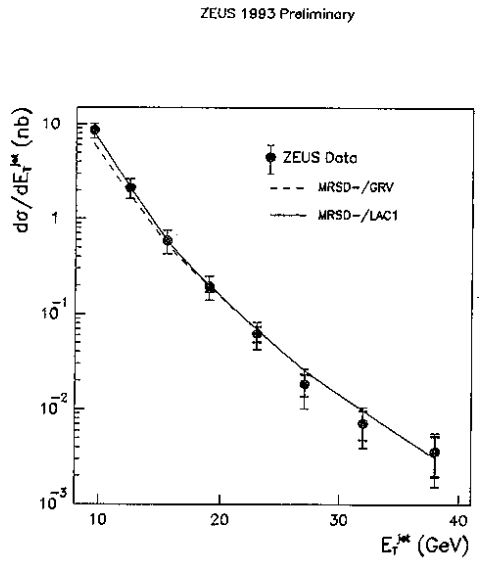

Figure 6: Measured differential cross section for inclusive jet production as a function of E_T^{jet} (black dots; thick error bars indicate the statistical errors of the data and MC used to calculate the corrections; thin error bars indicate the statistical and the systematic errors added in quadrature) compared to PYTHIA expectations including resolved and direct processes for two parametrizations of the photon parton distributions: GRV (dashed line) and LAC1 (solid line).

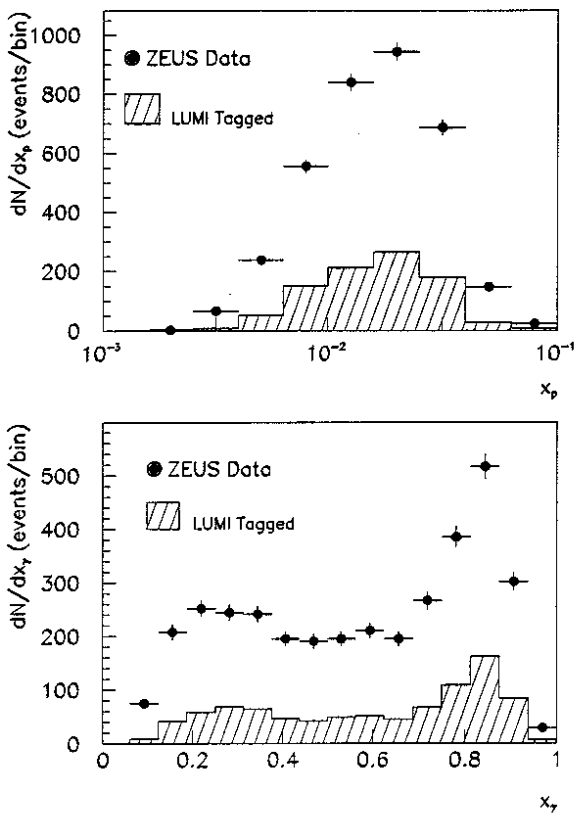

Figure 7: The computed fraction of momenta from the proton and the photon beams, x_p and x_γ, on the top and bottom, respectively. The peak at around 1 of x_γ corresponds to the direct processes where the photon scatters punctually on the parton coming from the proton. The x_p distribution shows that measurements of the gluon distribution are possible in the presently unknown region $x \leq 5 \cdot 10^{-3}$. The dashed zones corresponds to Lumi tagged events ($\approx 25\%$ of the total, well reproducing the global spectra).

a mass resolution of the order of $70 \div 80\ MeV/c^2$ and quite few background events (see fig. 8).

The D^* production is established through the Δm method, where Δm is the mass difference between the D^* and the D^0, in one of its more favorable decay channel. The mass difference ($\approx 145\ MeV/c^2$) peak is clearly seen, over a large increasing background, by both H1 and ZEUS (approximately 50 events are available, corresponding to half inverse picobarn of luminosity, for each experiment).

4 Conclusion

Three kind of conclusions can be depicted with respect to the photon behaviour at HERA. First, it is evident that HERA has proven to be able to distinguish between the different behaviours. By consequence the nature of the photon will be described in many aspects, the hadronic connection of the photon as well as its partonic one will be studied at 200 GeV of energy in the hard process center of mass. Second, the hard scattering of *quasi–real* photons will provide information on the proton constituents, in competition with the Deep Inelastic Scattering processes. The uniqueness of its direct measurement at small–x, expecially with reference to the gluonic component, is worthwhile. Third, we firmly believe that the 1994 data taking at HERA will be very profitable for the photon physics. The few inverse picobarn of luminosity that are going to be collected *will make the difference* in providing significant physical results.

References

[1] G. Schuler and T. Sjöstrand, Phys. Lett. B300 (1993) 169.

[2] H1 Collaboration, Phys. Lett. B328 (1994) 176

[3] ZEUS Collaboration, contributions to the Eilat Conference on Deep Inelastic Scattering, February 1994, and Contributed Paper to HEP Glasgow Conference, July 1994.

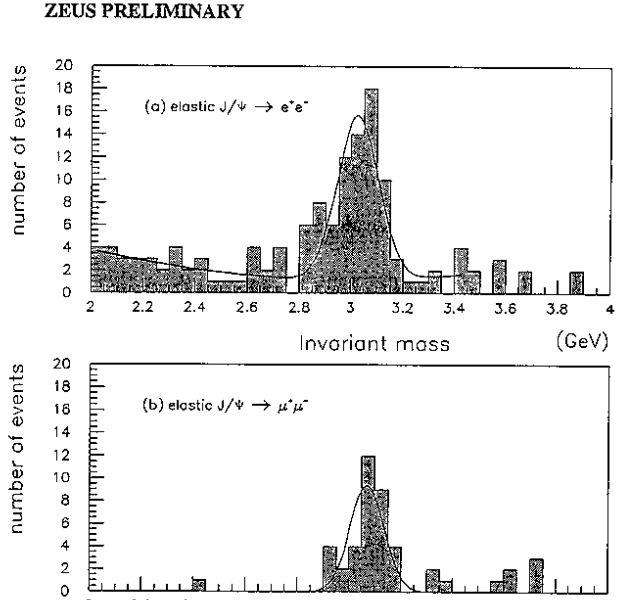

Figure 8: Invariant mass of J/ψ candidates from ZEUS experiment. The superimposed curves are in (a) a Gaussian and a second order polynomial, and in (b) a Gaussian.

[4] UA1 Collaboration, Nucl. Phys. B335 (1990) 261.

[5] OMEGA Photon Collaboration, Zeit. Phys. C43 (1989) 63.

[6] ZEUS Collaboration, Contributed Paper to HEP Glasgow Conference, July 1994.

[7] ZEUS Collaboration, Contributed Paper to HEP Glasgow Conference, July 1994.

[8] ZEUS Collaboration, DESY Internal Report 93–151, Accepted by Phys. Lett. *B*.

Partons in the Photon

R. Kaschowitz

III. Physikalisches Institut der RWTH Aachen, Germany

Introduction

At the ep collider HERA, the electron beam can be treated as a source of quasi-real photons colliding with protons. The electron is scattered through a small angle and therefore not observed in the main detector. These photoproduction events offer an excellent opportunity to study various aspects of the photon structure.

The photon itself can contribute to a hard partonic subprocess or it can fluctuate to quarks and then be treated as a source of quarks and gluons which give the input to the hard subprocess. The other input leg to the hard subprocess is a parton coming from the proton.

For the investigations discussed here, we look at the two cases of hard QCD subprocesses:
• direct processes: $\gamma g \longrightarrow qq$, $\gamma q \longrightarrow qg$
• resolved processes, e.g.: $qq \longrightarrow qq$, $gg \longrightarrow qq$, etc....
In a leading order process we expect to observe two jets in the HERA detectors coming from the two partons in the final state. Due to the asymmetric HERA kinematics, these jets are found mostly in the direction of the proton (forward direction). In addition there is a remnant jet from the proton (very forward direction) and a relatively soft remnant jet from the resolved photon processes (mainly backwards, the e^- direction).

We have measured inclusive jet rates for p_t and have unfolded these rates to a leading order parton cross section. This result can be compared with leading order QCD calculations of the hard subprocess including different assumptions of the photon structure function.

From the 2-jet events we can – knowing the photon energy – reconstruct and measure the distribution of x_γ, where x_γ is the part of the photon momentum which enters the hard subprocess. After unfolding it is possible to extract the leading order gluon density of the photon, as will be shown below.

Selection of hard scattering events

For the H1 detector [1] some aspects of data-taking and selection are considered here in more detail.

Data Selection

For photoproduction events one expects the scattering of the electrons at small angles. Therefore, a signal in the so-called electron detector, which is part of the luminosity system and which is placed outside the main detector in the backward direction, indicates a candidate for photoproduction. At H1 a coincidence from the electron tagger signal with a signal from at least one track of the central jet chamber ($p_t^{track} \geq 0.3GeV$) is used as a level-1 trigger condition for photoproduction events. The hard scattering selection is done during the analysis step looking for large calorimetric energies and jets. The energy of the scattered electron is measured with the tagging detector and – using the electron beam energy – the photon energy can be calculated. The e-tagger acceptance is known in the range $y\epsilon[0.2; 0.8]$ where $y = (E_{e^-}^{in} - E_{e^-}^{scatt})/(E_{e^-}^{in})$.
We summarize the data selection criteria:

- data from H1 run period 1993
- Integrated luminosity for this analysis: $\mathcal{L} = 290 \pm 5\% nb^{-1}$
- only e-tagged events were used with a trigger efficiency of $92\% \pm 2\%$ for the hadronic system.

Monte Carlo Properties

The MC comparisons with data and the corrections from the jets to the parton level is based on the PYTHIA generator [5]. For the correct description of the photon radiation a special photon generator H1IJRAY was added. Therefore PYTHIA is run in the γ-p mode. PYTHIA uses leading order QCD matrix elements including initial and final parton shower models. Furthermore the GRV structure functions were used in leading order for the proton and the photon [8], [9]; the scale was p_t. PYTHIA offers the possibility to switch on additional interactions between a parton of the photon remnant and a parton of the proton remnant. These so-called multiple interactions are indicated from proton-antiproton collisions. We have used the multiple interaction options with standard parameters. The hadronization was described by the JETSET fragmentation model. Finally, the generated events were simulated by a detailed detector simulation program and reconstructed with the same program as used for the data.

Jets

To avoid confusion the definition of the sign of the pseudo-rapidity η used by the HERA experimentalists should be mentioned here:
positive rapidities: the direction of the proton and its remnant:
$\longrightarrow$ the detector forward region
negative rapidities: the direction of the electron and the photon:
$\longrightarrow$ the detector backward region

In this analysis, jets are defined by a cone algorithm, based on [6], searching for calorimetric energy in the $\phi - \eta$-plane with an η range from $-3 < \eta < +3$. A cone jet is found if a certain p_t is exceeded within the cone radius $R = \sqrt{(\Delta\phi)^2 + (\Delta\eta)^2}$.
A jet is accepted for the analysis, if the jet axis is within the rapidity range of $\eta\epsilon[-0.5; 2.5]$. The other parameter values for the specific analysis are given here:
a. jet incl. spectrum: cone radius = 0.7, $p_t > 9$ GeV.
b. x_γ : cone radius = 1.0 (and 0.7), $p_t > 7$ GeV for two jets.

Unfolding Procedure

The correction of the data to parton level is based on the Monte Carlo correlations between reconstructed jets and parton quantities, see: fig. 2 and fig. 6. The unfolding procedure used by the H1 group was developed and coded by V.Blobel [7]. For a better understanding of the analysis here are some short remarks:

- The unfolding problem is a discrete problem for the unfolding quantity f. From MC events, a matrix A is defined by the mc generated-to-measured relation. The distribution of the generated quantity comes from an assumed model g_{gen}. Together with the measured data d a matrix equation is given and has to be solved: $d = A \cdot f$.
- Because all entries of the mc relation matrix A show statistical fluctuations, a regularization method has to be used for the inversion.
- The result of the inversion is a correction function f .This correction function f can be applied to the assumed mc model g_{gen} used during mc generation; this gives the true model $g_{true} = g_{gen} \cdot f$.
- An important feature of the method is a build-in check of the found true model. Every mc event is re-weighted by the correction function. By construction, the re-weighted distribution of the unfolded quantity itself now describes the data. The re-weighted distribution of several other quantities of the mc can be compared with the data distribution respectively. If these comparisons have no significant differences, the unfolding procedure worked.
- The method finds not only the correction function. In addition the resolution (bin sizes of the final result) and the correct statistical errors are determined.

This procedure is now applied to the p_t spectrum and to the x_γ distribution. Shown are the data compared to the mc distribution before and after re-weighting, several check quantities and the final result.

Inclusive Jet Cross Section

First, in fig. 3 a comparison is shown of the transverse energy p_t of the measured data to the original input and the unfolded mc spectrum. By construction, the unfolding method can correct for smearing, shape and shifts. Here a small shift is observed for the re-weighted mc after applying the unfolding. Second, we take a look at some test quantities (control plots). The re-weighted mc distributions (re-weighted due to the unfolding in p_t) fit the corresponding data distributions better than the original mc input distributions, which can clearly be seen in fig. 4. So we can apply the correction to the input mc model including the acceptance correction and look at the final result in fig. 5. Note that both partons are counted in this inclusive parton cross section.

The cross section is given for the acceptance region: $p_t \geq 9$ GeV, $y \epsilon [0.2; 0.8]$ and $\eta \epsilon [-0.5; 2.5]$. The resolution becomes worse with increasing p_t due to the small statistics for high pt jets. The comparison with the PYTHIA model using different parameterizations for the photon structure function shows that it is not possible to distinguish between the GRV and the LAC1 parameterization within the errors. A LAC3 type parameterization is ruled out within the errors. The systematic error is dominated by the uncertainty in the knowledge of the hadronic energy scale in the calorimeter. We show the shift coming from a $\pm 5\%$ variation of the jet p_t which corresponds to our present understanding of the energy scale of the calorimeter [2], [3], [4] together with the error of the trigger efficiency and the uncertainty of the luminosity measurement.

Gluon Density of the Photon

For the reconstruction of x_γ in a hard photoproduction event, the rapidities η_i and the transverse energies $p_{t,i}$ of two measured jets and the photon energy $E_\gamma = E_e \cdot y_{etag}$ are needed:

$$x_\gamma = \frac{1}{2E_e \cdot y_{etag}} \cdot (E_t^{jet1} \cdot exp(-\eta^{jet1}) + E_t^{jet2} \cdot exp(-\eta^{jet2}))$$

In. fig. 6 the mc correlation from the measured x_γ to the generator value is shown. The resolution is limited by the reconstruction of the jet p_t.

Before the unfolding procedure was applied, the differences of the jet pedestal in data and mc (see fig. 1) were taken into account: From a reconstructed jet we have subtracted a correction value $p_t^{corr.}$, which was constructed in terms of the rapidities of both jets of the event. Now the x_γ distribution was unfolded. After unfolding the mc spectrum has changed and describes the data obviously better, see fig. 7. Also the control plots in fig. 7 show, that the data are described better by the re-weighted mc events. For the control plots we took QCD quantities, which are related directly to the hard subprocess. The resulting x_γ spectrum is compared to the quark component of the photon (as measured in e^+e^- experiments, see [10]) together with the direct component (as known from QCD calculation and implemented in the PYTHIA monte carlo). In fig. 8 one can clearly see that at small x_γ values the spectrum cannot be explained by the quarks of the photon and the direct component. Gluons in the photon are needed to explain the x_γ spectrum at small x_γ !

In a leading order analysis we subtract the quark and direct part from the measured x_γ spectrum. The result is finally the leading order gluon density in the photon. The measured gluon density is shown in fig. 9. The inner error bars come from the statistical error, the outer include the known systematic effects:

- the uncertainty in the hadronic energy scale of the calorimeter of 5%.
- variation of the quark content in the photon by a factor of 0.5 and 2.0 relative to the GRV parameterization
- the uncertainty in the determination of the trigger efficiency
- the pedestal correction
- additional errors come from the luminosity measurement (5%, not shown in the figure)

We observe a small gluon density at large x_γ and see a clear rise towards small x_γ . This measurement is corroborated by an independent analysis using a smaller cone radius $R_{cone} = 0.7$ in the range $6 \cdot 10^{-2} < x_\gamma < 3 \cdot 10^{-1}$.

Conclusion

The HERA experiments are sensitive to the gluonic content of the photon. Within this contribution two important results are presented:

- We show the unfolded LO parton cross section for $\frac{d\sigma}{dp_t}|_{incl.}$. A LAC3 type structure function of the photon is ruled out.
- We measure the parton momentum fraction from the photon in 2-jet events. Using
  a) direct contributions known from QCD calculations and
  b) quark content in the photon as measured in e^+e^- experiments
  we extract a gluon density of the photon in LO.

References

[1] H1 Collab., I. Abt et al., "The H1 detector at HERA", DESY preprint 93-103 (1993), to be submitted to Nucl. Instr. and Meth..

[2] H1 Calorimeter Group, B. Andrieu et al., Nucl. Instr. and Meth. A336 (1993) 460.

[3] H1 Calorimeter Group, B. Andrieu et al., Nucl. Instr. and Meth. A336 (1993) 499.

[4] H.P. Wellisch et al., "Hadronic Calibration of the H1 LAr Calorimeter using Software Weighting Techniques", MPI-PhE/94-03, January 1994.

[5] T. Sjöstrand, CERN-TH-6488 (1992).

[6] J. E. Huth et al., Fermilab-Conf-90/249-E (1990).

[7] V. Blobel, DESY 84-118, and Proceedings of the 1984 CERN School of Computing, Aiguablava (Spain), CERN 1985.

[8] M. Glück, E. Reya and A. Vogt, Z. Phys. C53 (1992) 127.

[9] M. Glück, E. Reya and A. Vogt, Z. Phys. C53 (1992) 651.

[10] Opal Collab., R. Akers et al., Z. Phys. C61 (1994) 199.

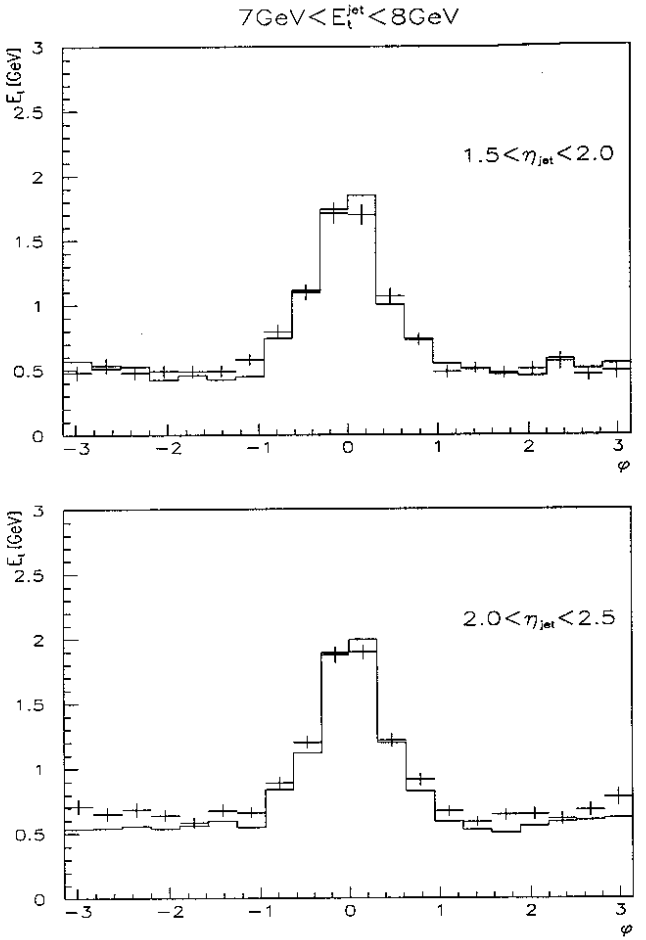

Figure 1: Shown are, in a slice of $|\Delta\eta| \leq 1$, the jet profiles in $\Delta\Phi$ for the mc (histogram) and for the data (crosses). In the upper plot the jet axis was found within an rapidity range from 1.5 to 2.0; the lower plot shows the situation for the rapidity bin of 2.0 to 2.5. Especially in the detector forward region mc and data jet profiles are different in the tails.

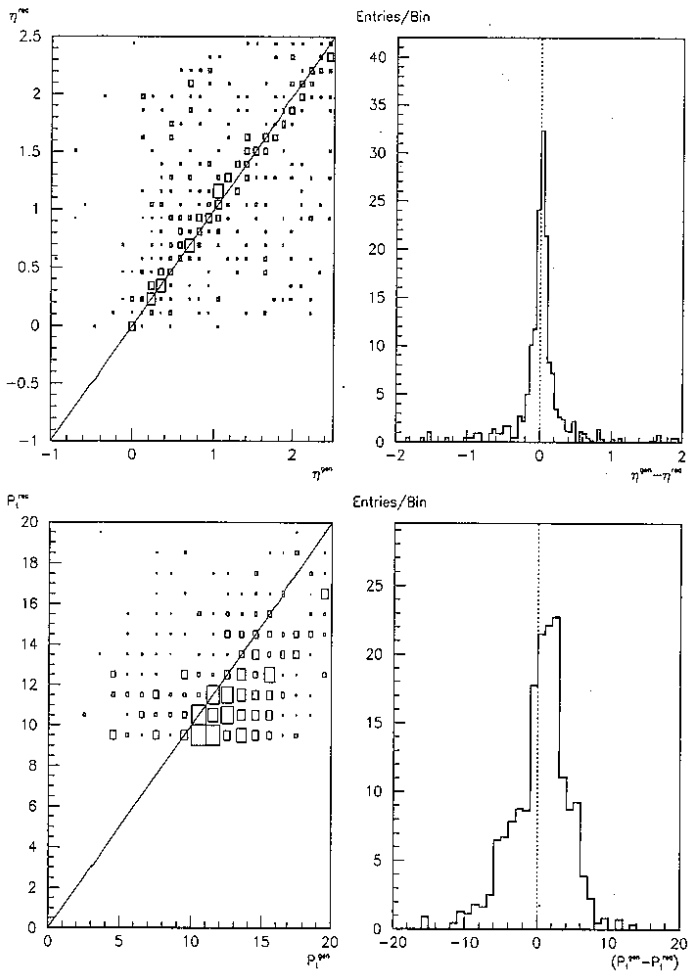

Figure 2: Monte Carlo: Correlation of jets and partons coming from the hard subprocess. Reconstruction of the parton rapidity is reasonable. The resolution in the reconstruction of the parton p_t is mainly influenced by the smearing of the calorimetric energy measurement.

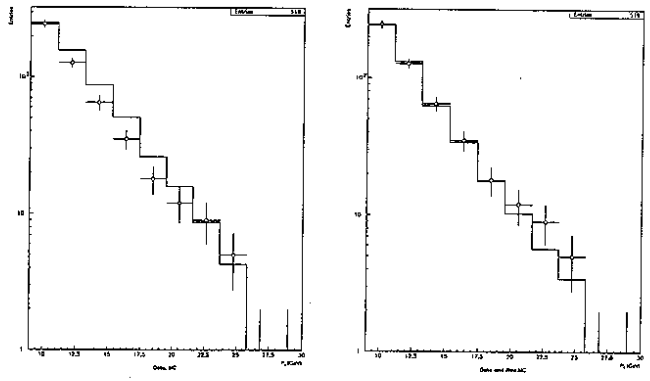

Figure 3: Shown is the correction effect of the unfolding of the p_t spectrum. The left plot shows data and mc before the method was applied. The correction of the mc is in this case mainly a shift.

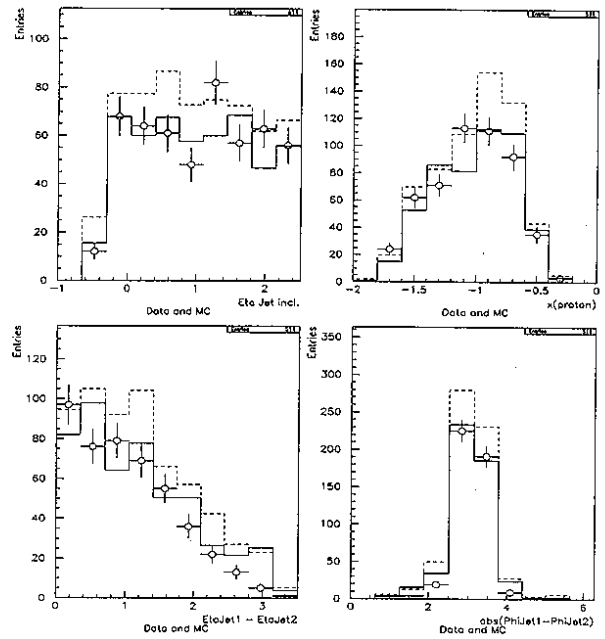

Figure 4: Control plots for the unfolding of p_t. Shown is the effect of the re-weighting of the mc events for quantities other than the unfolding quantity p_t.

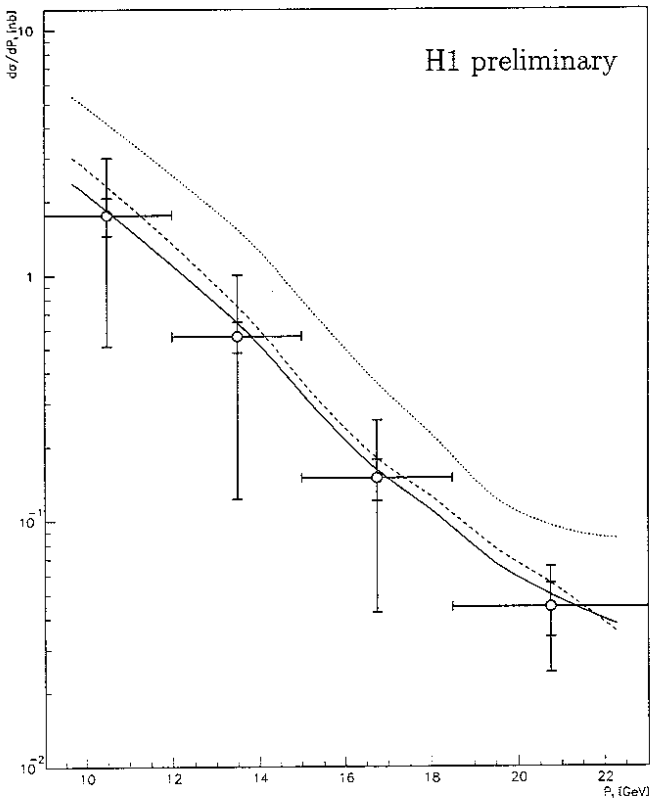

Figure 5: The unfolded p_t spectrum: Shown are the data points with the statistical errors (inner error bars) and in addition the systematic errors (outer error bars). For comparisons the smooth curves show the PYTHIA mc prediction assuming a GRV (full line), LAC1 (dashed line) and LAC3 (dotted line) gluon density of the photon.

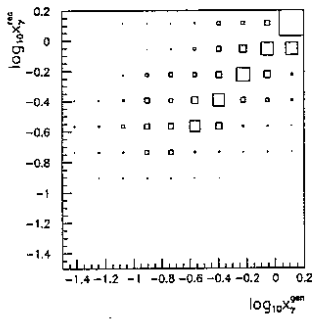

A study with the PYTHIA generator shows the correlation of the reconstructed x_γ and the generator values.

Figure 6: x_γ correlation

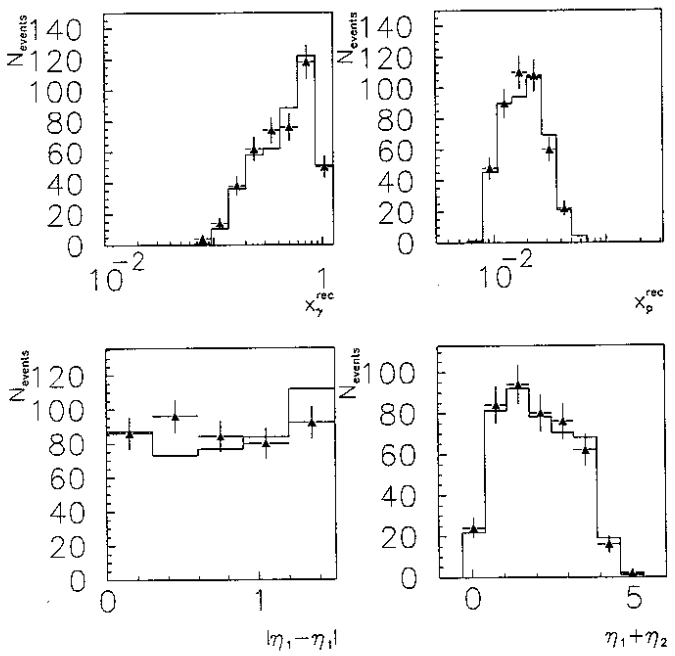

Figure 7: The unfolding of the x_γ distribution: shown are the result for x_γ itself and for some control quantities: x_{proton}, $|\eta_1 - \eta_2|$, $(\eta_1 + \eta_2)$. (solid lines: mc re-weighted by unfolding of x_γ).

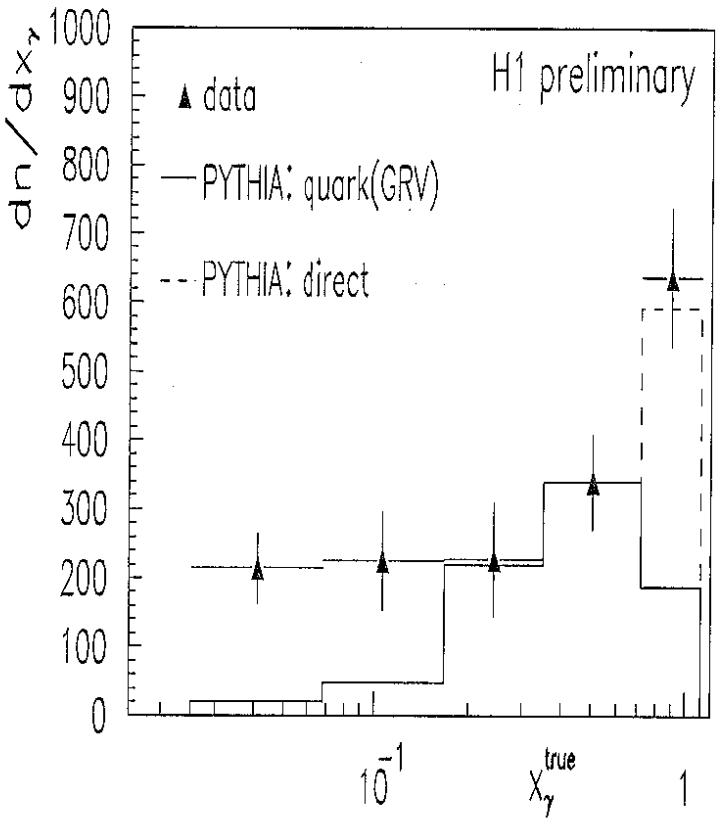

Figure 8: Using the unfolding method the measured x_γ distribution is corrected for the migrations to get the true value of x_γ (triangles). No correction for the detector acceptance or the analysis cuts were applied. The PYTHIA curve (solid line) contains the quark component of the photon and the dashed line indicates the direct contribution. This demonstrates that a gluon content in the photon is needed at small x_γ .

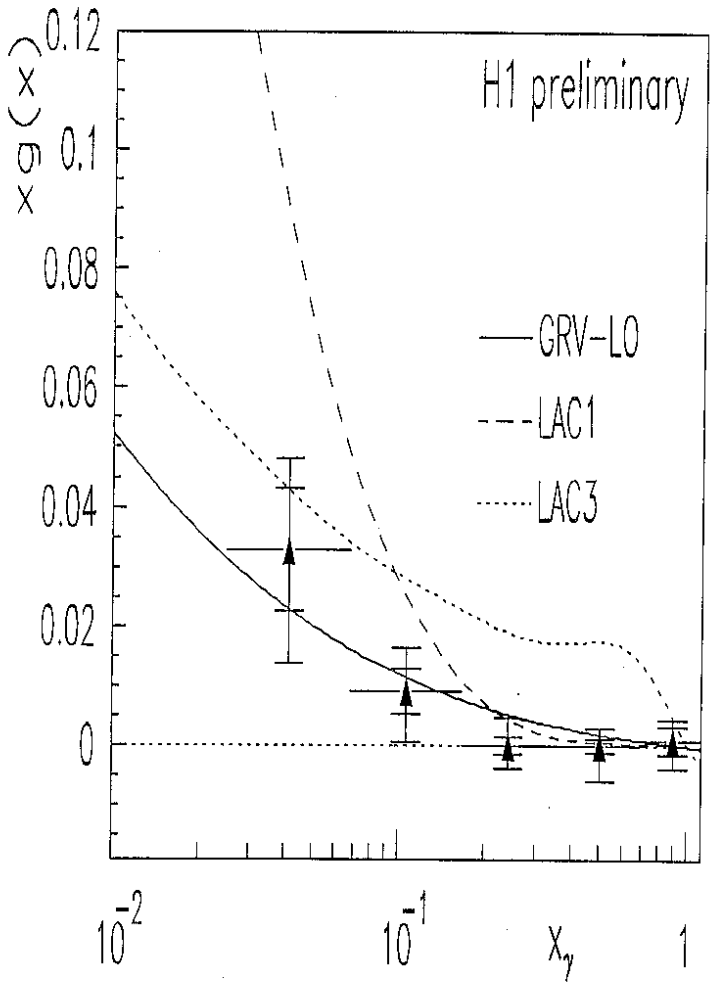

Figure 9: The measurement of the LO gluon density in the photon, compared to the GRV (solid line) and LAC1 (dashed line) structure function parameterizations at a scale of $60 GeV^2$.

Hard Scattering in Diffractive Dissociation of quasi-real Photons at HERA

Sergey Levonian
DESY, Hamburg, Germany and LPI, Moscow, Russia

Events with no hadronic energy flow in a large interval of pseudo-rapidity in the proton direction are observed by H1 and ZEUS collaborations in photon-proton interactions at the HERA collider. These events are interpreted as photon diffractive dissociation. Evidence for hard scattering in photon diffractive dissociation is presented from single particle spectra and jet production. The data can be described by a Monte Carlo including hard photon-Pomeron scattering.

1 Introduction

The electron-proton collider HERA has turned out to be an important research facility for the understanding of high energy photon-hadron interactions [1-5]. Quasi-real photons are produced in ep collisions by electrons which are scattered through small angles. In γp collisions centre-of-mass (CMS) energies up to 300 GeV can be reached. This is one order of magnitude larger than the CMS energies achieved so far in fixed target experiments.

One of the first important results obtained at HERA is a measurement of the total photoproduction cross section [6, 7] reviewed at this conference in [8]. It was found that like in hadron-hadron interactions, the γp total cross section rises weakly from the fixed target domain to HERA energies. As a result of this similarity, one expects a significant diffractive component in γp cross section. At this energy high mass diffractive dissociation processes in photoproduction can be studied. A salient feature of the diffractive events at high CMS energies is a gap in rapidity between the fragments of two interacting particles. Due to the asymmetry of the ep collisions HERA is especially suited to study the diffractive dissociation at the photon vertex, producing events well contained in the detectors. One can identify this class of events by requiring the absence of energy in the region of the HERA detectors in the proton direction. The diffractive events, which can be isolated by such a rapidity gap cut, are the sum of a single photon diffraction with a contamination of double diffraction, and are termed *photon diffraction* in the following.

Phenomenologically, the observed properties of the diffractive cross section are described by Regge theory where this process is viewed as the exchange of a Pomeron [9]. This model however gives no information on the details of the hadronic final states produced in diffractive dissociation. Traditionally the final state in diffraction is assumed to be described by a multiperipheral type of model with limited transverse momentum phase space. This approach was used so far for comparisons with the available measurements of multiplicity and rapidity distributions of charged particles from high mass diffractive states. On the other hand, in a modern QCD language, it is tempting to consider the Pomeron as a partonic system[10] which can be probed in a hard scattering process. Models based on this idea assume that the Pomeron essentially behaves as a hadron and the concept of a Pomeron structure function is introduced [11-14]. These models predict that, similar to high energy hadron-hadron scattering, jets and particles with large transverse momenta are produced in high mass diffractive dissociation. It was suggested that these hard hadron-Pomeron scattering events could be observed in diffractive hadronic collisions at high energies. Indeed, the UA8 collaboration recently has shown evidence for jet production in diffractive $\bar{p}p$ events [15], interpreted as resulting from the collisions with partons from the Pomeron. New data to study the partonic structure of the Pomeron are essential to establish this picture. In particular p_T spectra of particles and jet spectra are expected to provide an important information on the underlying dynamics of the diffractive process.

This contribution summarises first observation of events with a rapidity gap in photoproduction at HERA. Based on the comparison with MC calculations these events are interpreted as photon diffractive dissociation. The events exhibit hard scattering properties comparable to the full γp data. The analysis was performed on data collected in 1993 with the H1 and ZEUS detectors at HERA, for collisions of e and p beams with energies of 26.7 GeV and 820 GeV respectively.

2 Data Samples and Monte Carlo Models

A general description of the H1 and ZEUS detectors is given in [16]. The data used in the present analysis by the two experiments are only partially overlapping in the kinematical range and complementary to each other. H1 used so-called *minimum bias tagged* events in which the energy of the small angle scattered electron was measured in the electron calorimeter of the H1 luminosity system. This limits the acceptance for the incident photons to the kinematical range of $3 \times 10^{-8}\text{GeV}^2 < Q^2 < 10^{-2}\text{GeV}^2$ and $0.25 < y < 0.7$, where $y = 1 - E'/E$, E and E' are the energies of the incoming and scattered electron respectively. A coincidence of the small angle electron detector signal ($E' > 4$ GeV) with at least one track of $p_T \gtrsim 150$ MeV/c pointing to the vertex region was used to trigger these events. The acceptance of such a trigger was studied in [7].

In contrast, ZEUS selected *untagged* γp events by requiring no electron detected in the main calorimeter. This corresponds to the larger range of $Q^2 \lesssim 2$ GeV^2 and the available energy interval of the $\gamma^* p$ system 70 GeV $< W <$ 270 GeV. A minimum transverse energy of the event, E_T, of 5 GeV was used as a trigger condition. Throughout this paper the transverse energy is defined with respect to the beam axis.

Global characteristics of the both data samples are summarized in table 1. For the quantitative comparison, it is important to note a somewhat larger acceptance of the ZEUS detector for the final hadronic system M_X.

Table 1: Comparison of the H1 and ZEUS data used in present analysis

Detector	Q^2_{max} [GeV^2]	E_{Tmin} [GeV]	$W_{\gamma^* p}$ [GeV]	$\mathcal{L}$ [nb^{-1}]	Statistics [events]	$\eta_{max} < 1.5$ All E_T	$\eta_{max} < 1.5$ $E_T > 5$ GeV	η range for M_X
H1	0.01	~ 0.2	$150 \div 250$	290	320 000	14 200	4160 (1.3%)	[-3.4, +3.6]
ZEUS	~ 2.0	5.0	$70 \div 270$	550	417 000		6678 (1.6%)	[-3.8, +4.3]

In the following the uncorrected H1 and ZEUS data will be compared with Monte Carlo predictions which were simulated through the corresponding detector and reconstructed as for the real data. All figures are shown with statistical errors only.

Soft hadronic events were generated with the PYTHIA 5.6 [18] Monte Carlo event generator in the photon-hadron option, which includes the diffractive components of the cross section. The diffraction is modelled following well known properties of soft peripherial hadronic dissociation [9]: an exponential t dependence and a $1/M_X^2$ behaviour of the cross section and the fragmentation of the diffractive system M_X according to the longitudinal phase space configuration. Here t is the four momentum transfer between the interacting beam particles. This model, though technically based on a partonic picture, does not include hard scattering between partons of the photon and the proton or Pomeron and will be refered to as the *soft diffractive model*.

For further study, a model is used which explicitely includes *diffractive hard scattering*: POMPYT [20]. This model proceeds by the emission of a Pomeron at the proton vertex with a small momentum transfer. The resulting photon-Pomeron interaction is simulated as a hard scattering of the partons in the photon and exchanged Pomeron, according to leading order QCD calculations for the hard scattering processes. These collisions can lead to the production of particles with large p_T and jets.

To compare with non-diffractive hard scattering in photon-hadron interactions, the generator PYTHIA 5.6 was used in its high p_T option for photoproduction. The simulation of the γp collisions is based on leading order QCD matrix elements for the hard scattering processes, while the effects of initial and final state QCD radiation are described by leading logarithm type parton showers. Multiple parton interactions were included. This model will be refered to as the *non-diffractive model* in the following. It was shown to describe the basic features of the full γp data [3, 4].

In both the high p_T PYTHIA and POMPYT models a minimum p_T cut-off value of $\hat{p}_T^{min} = 2$ GeV/c was used for the transverse momentum of the outgoing partons in the hard scattering process. For the structure functions, the GRV leading order parametrizations for both the proton [21] and the photon [22] are used. In this analysis the Pomeron was assumed to consist of gluons and their distribution function within the Pomeron was taken to be either "hard", $zg(z) = 6z(1-z)$, or "soft", $zg(z) = 6(1-z)^5$, where z is the fraction of the Pomeron's momentum carried by the gluon involved in the interaction.

3 Rapidity Gap Events

The energy flow in the selected events was investigated using the variable η_{max}, the pseudorapidity of the most forward calorimetric energy deposit of 400 MeV or of the detected track with a transverse momentum $p_T > 0.150$ GeV/c. The η_{max} spectrum is shown in fig. 1 for the H1 minimum bias sample of γp events. In addition to the bulk of the events populating the area close to the high end of the η_{max} spectrum, there is also a class of events with small η_{max} value, i.e. a large empty region in the calorimeter around the proton direction. This observation does not change by varying the minimum cluster energy and track p_T requirements by 30%.

The η_{max} spectrum can be qualitatively understood by comparing it with model predictions for diffractive and non-diffractive events.

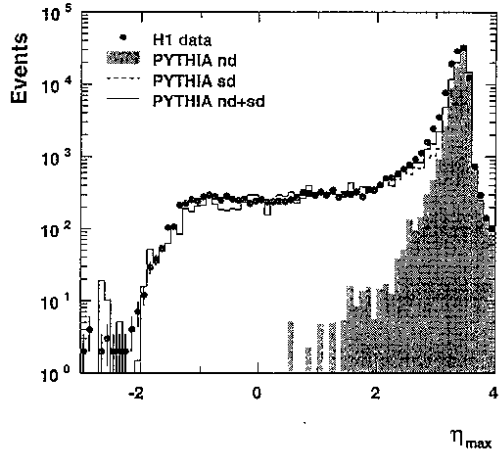

Figure 1: Maximum pseudo-rapidity distribution in γp events compared to Monte Carlo predictions, explained in the text.

Monte Carlo distributions in fig. 1 show that the events with small η_{max} can be identified with photon diffractive dissociation. The non-diffractive prediction (PYTHIA ND) exhibits an exponential fall off with increasing gap size, i.e. decreasing η_{max} and clearly does not account for the tail at $\eta_{max} < 2$. The photon diffractive component (PYTHIA SD) as predicted by the soft diffractive model gives a good description of the spectrum for $\eta_{max} < 2$. The shape of η_{max} distribution for the events with a rapidity gap is determined by the $1/M_X^2$ behaviour of the diffractive cross section, as implemented in the MC model. Note that in fig. 1 the SD distribution is normalised to the region $\eta_{max} < 1$, while the ND distribution is normalised to $\eta_{max} > 3$.

In all, the sum of the soft diffractive and non-diffractive γp Monte Carlo (full line) accounts well for the observed η_{max} spectrum.

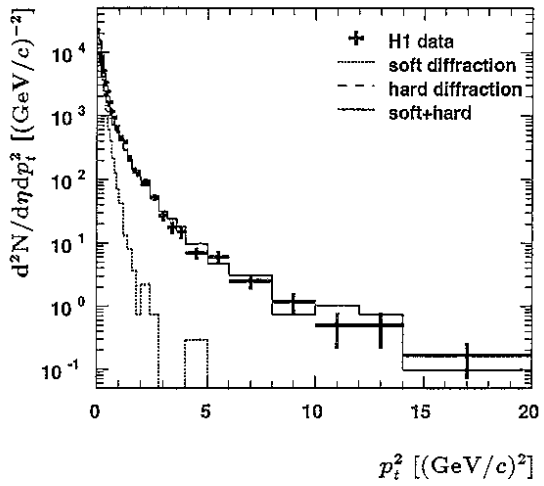

Figure 2: Transverse momentum squared distribution of charged particles in the events with large pseudo-rapidity gap (η_{max} <1.5) compared to Monte Carlo predictions explained in the text.

The events with $\eta_{max} < 1.5$ have been selected to study the properties of the rapidity gap events. In fig. 2 the p_T^2 spectrum for charged tracks in the range $-1.5 < \eta < 1.5$ is shown, where p_T is measured with respect to the beam axis. The distribution shows an exponential fall off at small p_T^2 values with a large tail extending to $p_T^2 \sim 20$ GeV^2. This is similar to the p_T spectra measured in the full photoproduction sample [3], where the events in this tail were identified with hard scattering in γp interactions. Similarly, the data are compared with the soft diffractive model prediction from PYTHIA (dotted line) and the hard diffractive model predictions of POMPYT (dashed line). The latter gives a satisfactory description of the large p_T region, which signals the occurance of the hard scattering at the parton level in the photon diffraction.

Note that, as seen from fig. 1, the contribution to the p_T spectrum of the remaining hard non-diffractive events in the rapidity gap sample is negligibly small.

4 Jets in Diffractive Photoproduction

To substantiate the above evidence for hard scattering, a search was made for jet structures in both H1 and ZEUS data samples of large rapidity gap events ($\eta_{max} < 1.5$) with transverse energy larger than $5\,GeV$ (see table 1). A cone algorithm with radius $R = 1.0$ in the space of pseudorapidity η and azimuth ϕ was applied to search for jets. A detailed description of the algorithm can be found elswhere [17, 16]. Cones with $E_T > 4$ GeV and $\eta_{jet} < 1.5$ were accepted as jets in this analysis.

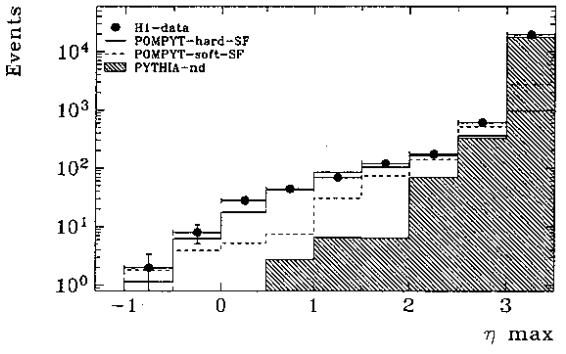

Figure 3: Maximum pseudo-rapidity distribution in H1 tagged γp events containing jets with E_{Tjet} >4 GeV in -1.0 < η_{jet} < 1.5 interval, compared to Monte Carlo expectations

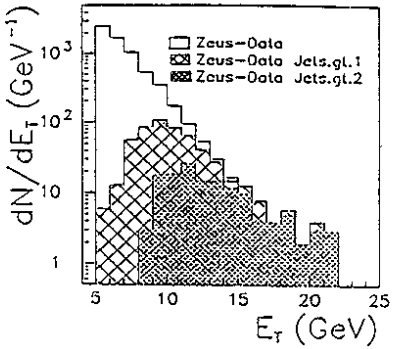

Figure 4: Transverse energy distribution for the large pseudo-rapidity gap events ($\eta_{max} < 1.5$) in ZEUS detector

The η_{max} distribution for all H1 γp events with $E_T > 5$ GeV containing at least one jet is shown in fig. 3. Similar to the distribution in fig. 1 a clear signal of events with $\eta_{max} < 2$ is observed. Hence, the diffractive candidates exhibit jet features similar to the non diffractive γp data. The fall off of the spectrum for $\eta_{max} < 1$ results from the reduction of the available phase space for jet production. Indeed, the η_{max} cut is strongly correlated with M_X, the hadronic mass of the diffractively produced system. Requiring η_{max} to be small preferably selects small M_X events, which have less phase space for the production of jets. The η_{max} data are compared with non-diffractive hard scattering γp (PYTHIA) and γ-Pomeron (POMPYT) predictions. The non-diffractive γp prediction, when normalized to the largest, η_{max} bin, cannot account for the η_{max} at small values. The POMPYT model accounts better for the shape of the η_{max} spectrum. with a slight preference for the configuration including a hard gluon distribution for the Pomeron.

Fig. 4 shows, that jets with $E_T > 4$ GeV are observed almost in all rapidity gap events with E_T above 10 GeV. Jet profiles, shown in fig. 5, are observed to be very similar in diffractive-like events ($\eta_{max} < 1.5$) and non-diffractive events ($\eta_{max} > 2$), with the exception of the large $\Delta\eta$ region ($1 < \Delta\eta < 2$). This corresponds to the region required to be devoid of energy in the rapidity gap selection. The hard diffractive scattering Monte Carlo POMPYT describes the rapidity gap event jet profiles well.

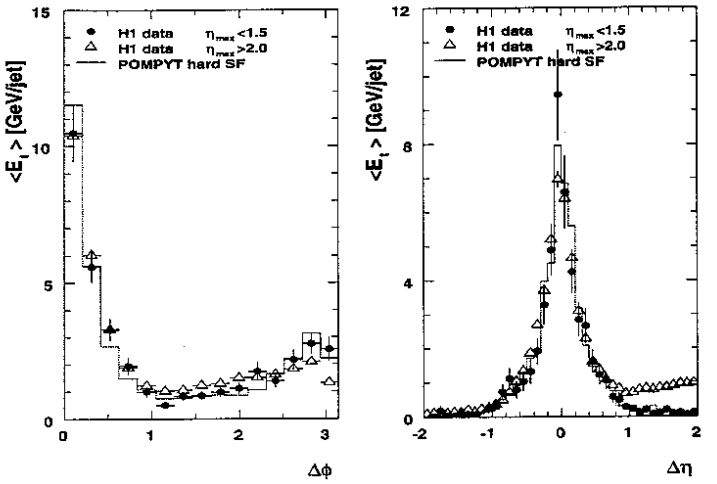

Figure 5: Jet profiles of 4 GeV < E_{Tjet} < 6 GeV jets with $\eta_{jet} < 0.5$

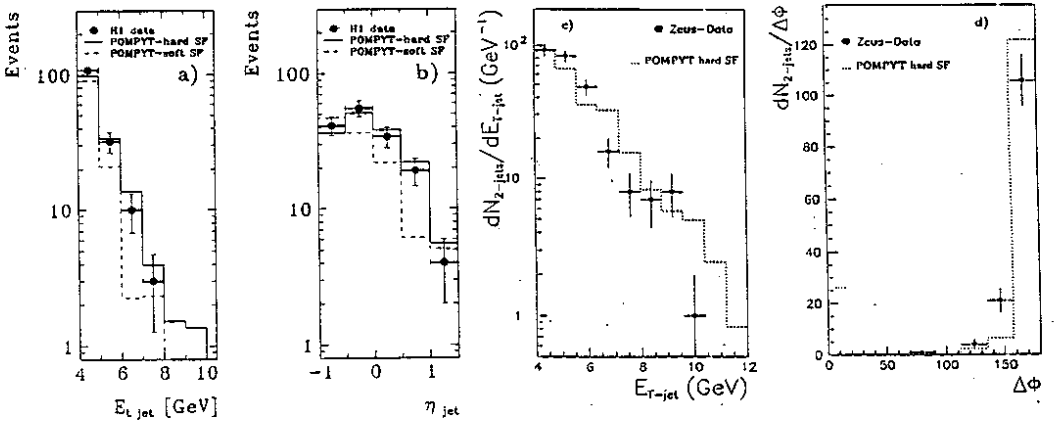

Figure 6: Inclusive jet distributions for large pseudo-rapidity gap events (η_{max} <1.5). $\Delta\phi = |\phi_{j1} - \phi_{j2}|$

Shown in fig. 6 inclusive jet distributions in all (a,b) and two jet (c,d) events are also in a good agreement in shape with POMPYT predictions. With the present statistics there is no clear preference for one or the other parton distribution in the Pomeron.

The relative fractions of jet events with different jet multiplicities w.r.t. to the total number of H1 and ZEUS events with $E_T > 5$ GeV are given in table 2. Both experiments are in a good agreement, taking into account the difference in the diffractive sample selections explained in section 2. Jet rates

in H1 rapidity gap events are also compared in table 3 with POMPYT predictions. In this case to enhance hard scattering region, at least 6 GeV E_T was required for the event. The 1- and 2-jet fractions are then 11.8% and 2.4% respectively. The ratio of (2-jet)/(1-jet) events is 0.20 ± 0.05 and compares favourably with the prediction of the hard Pomeron structure function, but it should be noted that this ratio depends somewhat on the choice of the $\hat{p}_T^{min}$ value. Note also that the absolute jet rates can be different from the data since we expect still a soft component to be present in the data and absent in POMPYT Monte Carlo.

Table 2: Jet rates in γp events with $E_T > 5$GeV and $\eta_{max} < 1.5$, and for jets with $E_{Tjet} > 4$ GeV and $-1 < \eta_{jet} < 1.5$

No of jets	H1	ZEUS
0	91.4%	91.4%
1	7.2%	6.5%
2	1.4%	2.0%
≥ 3	-	0.1%

Table 3: Jet rates: H1 data compared to POMPYT Monte Carlo ($\hat{p}_T^{min} = 2$GeV/c), for γp events with $E_T > 6$GeV and $\eta_{max} < 1.5$, and for jets with $E_{Tjet} > 4$GeV and $-1 < \eta_{jet} < 1.5$

Sample	All events	1 jet ev. (%)	2 jet ev. (%)	Ratio 2-j/1-j
H1 data	1003	11.8	2.4	0.20 ± 0.05
POMPYT hard SF	1726	21.6	3.6	0.17 ± 0.02
POMPYT soft SF	359	9.5	-	< 0.03

Both the inclusive p_T spectrum and the jet analysis turn out to be compatible with the ansatz of hard scattering between partons of the photon with partons of the Pomeron, as e.g. implemented in POMPYT.

5 Conclusions

HERA provides, in many aspects an unique, opportunity for a rich study program of diffractive phenomena. Events with a large rapidity gap with respect to the proton direction are observed in photoproduction at HERA. The gross features of these events are consistent with diffractive dissociation of the photon. In addition, diffractive events isolated by using a $\eta_{max} < 1.5$ cut show evidence for the hard scattering. The transverse momentum distribution of charged particles in these events demonstrates a large p_T^2 tail, which is not accounted for by a conventional model containing only soft peripherial interactions. A model including hard scattering between partons of the proton and the Pomeron shows the same behaviour as the data. Jets with transverse energy up to 10 GeV were found in both H1 and ZEUS diffractive data samples, substantiating the evidence for hard partonic scattering in diffractive γp collisions. H1 and ZEUS experiments are at the very beginning of this interesting program: more results are expected soon, using proton tagging by Roman Pots and exploiting a full capability of the detectors to tag gaps in larger η intervals.

References

[1] H1 Collab., T. Ahmed *et al.*, Phys. Lett. B 297 (1992) 205.

[2] H1 Collab., I. Abt *et al.*, Phys. Lett. B 314 (1993) 436.

[3] H1 Collab., I. Abt *et al.*, Phys. Lett. B 328 (1993) 176.

[4] ZEUS Collab., M.Derrick *et al.*, Phys. Lett. B 297 (1992) 404.

[5] ZEUS Collab., M.Derrick *et al.*, Phys. Lett. B 322 (1994) 287.

[6] ZEUS Collab., M. Derrick *et al.*, Phys. Lett. B 293 (1992) 465.
ZEUS Collab., M. Derrick *et.al.*, DESY 94-032 (1994).

[7] H1 Collab., T. Ahmed *et al.*, Phys. Lett. B 299 (1993) 374.
S. Levonian, Low and Medium $p \perp$ Photoproduction at HERA, in DESY 93-077 (1993).

[8] B.Burow, Results from the ZEUS and H1 Experiments at HERA on the Total Photoproduction Cross Section and its Contributions, in these proceeedings.

[9] K. Goulianos, Phys. Rep. 101 (1983) 169.

[10] F.F. Low, Phys. Rev. D 12 (1975) 163. S. Nussinov Phys. Rev. Lett. 34 (1975) 1268.

[11] G. Ingelman, P.Schlein, Rhys. Lett. B152 (1985) 256.

[12] A.Donnachie and P.V.Landshoff, Phys Lett. B191 (1987) 309.

[13] N.N.Nikolaev and B.G. Zakharov, Z.Phys. C53 (1992) 331

[14] J. D. Bjorken, "Hadron Final States in Deep Inelastic Processes", in "Current Induced Reactions: International Summer Institute in Theoretical Particle Physics in Hamburg 1975", ed. J. G. Kröner, G. Kramer, and D. Schildknecht, Lecture Notes in Physics, Springer Verlag, 1976.

[15] UA8 Collab., R. Bonino, et al., Phys. Lett. B211 (1988) 239.

[16] M.Erdmann, in these proceeedings.

[17] J.E. Huth et al., *Towards a Standardization of Jet Definitions*, Fermilab Conf 90/249-E (1990).

[18] T.Sjöstrand and M.Bengtsson, Comp. Phys. Comm. 43 (1987) 367;
H.-U.Bengtsson and T.Sjöstrand, Comp. Phys. Comm. 46 (1987) 43;
T.Sjöstrand, CERN-TH-6488 (1992).

[19] E612 Collab., T.J. Chaplin, et al., Phys. Rev. D31 (1985) 17.

[20] G. Ingelman, to be published.

[21] M. Glück, E. Reya and A. Vogt, Z. Phys. C 53 (1992) 127.

[22] M. Glück, E. Reya and A. Vogt, Phys. Rev. D 46 (1992) 1973.